1991-12

Computer analysis of harmonic distortion in electrical power distribution systems.

Gedo, Christopher N.

Monterey, California. Naval Postgraduate School

NAVAL POSTGRADUATE SCHOOL
Monterey, California

THESIS

Computer Analysis of Harmonic Distortion
in
Electrical Power Distribution Systems

by

Christopher N. Gedo

December 1991

Thesis Advisor: Stephen M. Williams

Approved for public release; distribution is unlimited

REPORT DOCUMENTATION PAGE

Form Approved
OMB No 0704-0188

1a REPORT SECURITY CLASSIFICATION UNCLASSIFIED	1b RESTRICTIVE MARKINGS
2a SECURITY CLASSIFICATION AUTHORITY	3 DISTRIBUTION / AVAILABILITY OF REPORT Distribution is unlimited
2b DECLASSIFICATION / DOWNGRADING SCHEDULE	
4 PERFORMING ORGANIZATION REPORT NUMBER(S)	5 MONITORING ORGANIZATION REPORT NUMBER(S)
6a NAME OF PERFORMING ORGANIZATION Naval Postgraduate School 6b OFFICE SYMBOL (If applicable) EC	7a NAME OF MONITORING ORGANIZATION Naval Postgraduate School
6c ADDRESS (City, State, and ZIP Code) Monterey, CA 93943-5000	7b ADDRESS (City, State, and ZIP Code) Monterey, CA 93943-5000
8a NAME OF FUNDING SPONSORING ORGANIZATION 8b OFFICE SYMBOL (If applicable)	9 PROCUREMENT INSTRUMENT IDENTIFICATION NUMBER
8c ADDRESS (City, State, and ZIP Code)	10 SOURCE OF FUNDING NUMBERS PROGRAM ELEMENT NO / PROJECT NO / TASK NO / WORK UNIT ACCESSION NO

11 TITLE (Include Security Classification)
COMPUTER ANALYSIS OF HARMONIC DISTORTION IN ELECTRICAL POWER DISTRIBUTION SYSTEMS

12 PERSONAL AUTHOR(S)
GEDO, Christopher N.

13a TYPE OF REPORT	13b TIME COVERED	14 DATE OF REPORT (Year, Month, Day)	15 PAGE COUNT
Master's Thesis	FROM _____ TO _____	December 1991	63

16 SUPPLEMENTARY NOTATION
The views expressed in this thesis are those of the author and do not reflect the official policy or position of the Department of Defense or the US Government.

17 COSATI CODES			18 SUBJECT TERMS (Continue on reverse if necessary and identify by block number)
FIELD	GROUP	SUB-GROUP	Harmonics, Distribution, Converter, Rectifier, Power, Distortion

19 ABSTRACT (Continue on reverse if necessary and identify by block number)

The number of nonlinear loads connected to power distribution systems is rapidly increasing. These loads disturb the sinusoidal nature of the power distribution systems to which they are connected. Consequently, all connected loads may be affected by even a single nonlinear load. This makes power quality an increasingly important issue, particularly in shipboard applications because equipment malfunction can cause the loss of life.

This study primarily develops a modeling technique for use with the harmonic power flow program (HARMFLO) developed by the Electric Power Research Institute. A land based power distribution system is modeled and simulation results are compared to field measurements. Additionally, the causes and effects of harmonic disturbances in power distribution systems are reviewed.

In spite of the fact that many parameters of the system being modeled are not

20 DISTRIBUTION / AVAILABILITY OF ABSTRACT	21 ABSTRACT SECURITY CLASSIFICATION	
☒ UNCLASSIFIED/UNLIMITED ☐ SAME AS RPT ☐ DTIC USERS	UNCLASSIFIED	
22a NAME OF RESPONSIBLE INDIVIDUAL WILLIAMS, Stephen M.	22b TELEPHONE (Include Area Code) (408) 646-3001	22c OFFICE SYMBOL EC/Wl

19. cont.
precisely known, simulation results are similar to the field measurements. This implies that HARMFLO has applications in isolating existing harmonic disturbances of installed systems and impact assessment for planned systems with one or more nonlinear loads.

Approved for public release; distribution is unlimited.

Computer Analysis of Harmonic Distortion in Electrical Power Distribution Systems

by

Christopher N. Gedo
Lieutenant, United States Naval Reserve
B.E.E., University of Minnesota, 1983

Submitted in partial fulfillment of
the requirements for the degree of

MASTER OF SCIENCE IN ELECTRICAL ENGINEERING

from the

NAVAL POSTGRADUATE SCHOOL
December 1991

ABSTRACT

The number of nonlinear loads connected to power distribution systems is rapidly increasing. These loads disturb the sinusoidal nature of the power distribution systems to which they are connected. Consequently, all connected loads may be affected by even a single nonlinear load. This makes power quality an increasingly important issue, particularly in shipboard applications because equipment malfunction can cause the loss of life.

This study primarily develops a modeling technique for use with the harmonic power flow program *(HARMFLO)* developed by the Electric Power Research Institute. A land based power distribution system is modeled and simulation results are compared to field measurements. Additionally, the causes and effects of harmonic disturbances in power distribution systems are reviewed.

In spite of the fact that many parameters of the system being modeled are not precisely known, simulation results are similar to the field measurements. This implies that *HARMFLO* has applications in isolating existing harmonic disturbances of installed systems and impact assessment for planned systems with one or more nonlinear loads.

TABLE OF CONTENTS

I. INTRODUCTION

A. OVERVIEW

All ships and aircraft in the United States Navy have ac power distribution systems installed. Each of these systems is subjected to loads that produce disturbances in the system current flow. Some of these disturbances are referred to as *harmonic* currents and can cause equipment malfunction, power loss, and even catastrophic equipment failure [1]. Therefore, a tool is needed to assess the impact of harmonic producing loads on power distribution systems.

The Electric Power Research Institute (EPRI) produced a harmonic flow computer program called *HARMFLO*. Power distribution systems can be modeled and simulated with this program. Since its development in the early 1980's, *HARMFLO* has not been exhaustively tested and compared to field data on power distribution systems [2:pp. 1–2]. As a result, the effects of program limitations and accuracy are not quantitatively known. If the accuracy of *HARMFLO* is documented, program simulations may be used to isolate existing problems with installed equipment and to estimate the impact of proposed harmonic producing loads on power distribution systems [3].

This study develops a power distribution system modeling technique for use with *HARMFLO*. A land based power distribution system is modeled in detail and extensively simulated. Many details about the system are not known precisely; much of the modeling process involves making assumptions and estimating system parameters. This lack of specific system information is consistent with other studies of power distribution systems. Simulation results are compared to field measurements and conclusions drawn about program accuracy and limitations. Additionally, *HARMFLO* output is

compared with current military power quality guidance; comments about the applicability of such comparisons are provided.

B. THE FIELD STUDY

1. The System

The system under test is the Union Electric Audrain County 12 kV distribution system. A number of residential, commercial, and industrial loads are connected to the distribution system. One industrial load, hereafter referred to as the customer, operates seven 100 HP adjustable speed DC drives. Additionally, there are six capacitor banks installed throughout the system. A one-line drawing of the Audrain County subsystem is shown in Fig. 1. [4]

The system connections shown in Fig. 1 are modeled as transmission lines. Impedances are taken from the utility database and are expressed as a percentage of the system impedance base [4]. The system impedance base is defined as

$$Z_B = \frac{\left(V_{B(l-l)}\right)^2}{S_{B(3\Phi)}}, \tag{1.1}$$

where $V_{B(l-l)}$ is the base line to line voltage in kV and $S_{B(3\Phi)}$ is the three phase system power base in MVA [5:pp. 32]. The system power base is 100 MVA with a voltage base of 12.5 kV [4]. Therefore, the system impedance base is

$$Z_B = \frac{(12.5\,\mathrm{kV})^2}{100\,\mathrm{MVA}} = 1.56\,\Omega \tag{1.2}$$

and the system current base is

$$I_B = \frac{S_{B(3\Phi)}}{\sqrt{3}\,V_{B(l-l)}} = \frac{100\,\mathrm{MVA}}{\sqrt{3}\,12.5\,\mathrm{kV}} = 4619\,\mathrm{A}. \tag{1.3}$$

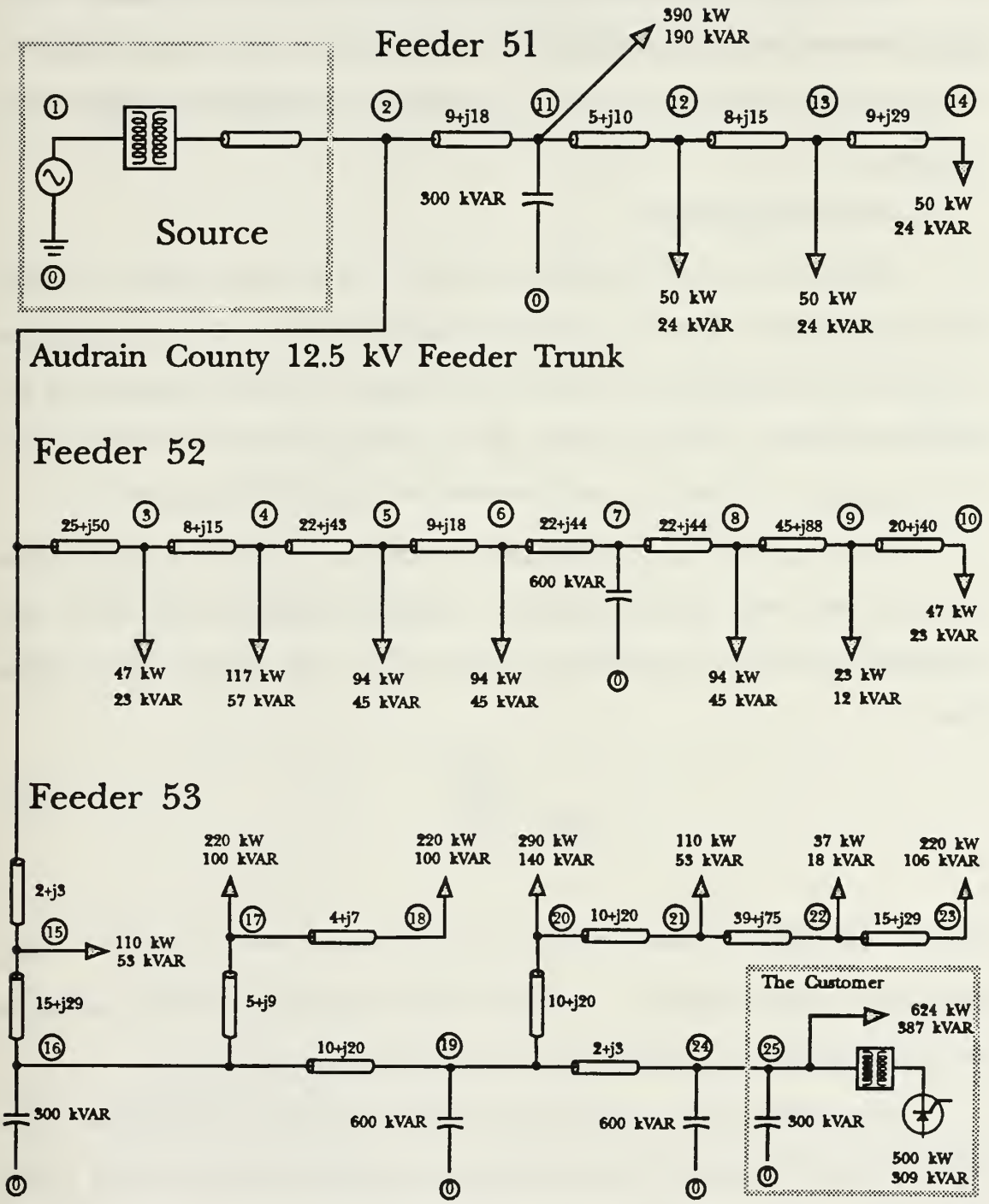

Fig. 1: One-line drawing of the Union Electric Audrain County 12 kV distribution system

The loads are estimated from utility data and are based on an assumed 0.9 lagging power factor except for the customer, whose assumed power factor is 0.85 [4]. The procedures used to model the loads and source are presented with greater detail in Chapter IV.

2. Field Measurements

Harmonic levels of the system under test were measured on May 18, 1990. That study, hereafter referred to as the field study, measured RMS current and potential levels of the fundamental, third, fifth, and seventh frequency components at two subsystem locations. Nodes two and 24 of Fig. 1 were the measurement points and V_2, $I_{1\text{-}2}$, $I_{2\text{-}11}$, $I_{2\text{-}3}$, $I_{2\text{-}15}$, V_{24}, and $I_{24\text{-}25}$ were recorded for the indicated harmonics. [4]

The voltage and current total harmonic distortion (THD) were both measured directly at node two; however, because of equipment limitations THD values were computed from the other measurements at node 24. [4] The voltage THD is defined to be

$$THD = \frac{\sqrt{\sum_{i=2}^{\infty} V_i^2}}{V_1} \tag{1.4}$$

where V_1 is the RMS magnitude of the voltage fundamental and V_i is the RMS magnitude of the i^{th} voltage harmonic. The current THD is defined the same way except that the voltage quantities are replaced by their current counterparts. [6:pp. 8]

Measurements were recorded for six different subsystem configurations. First, all five subsystem capacitor banks external to the customer at nodes 24, 19, 16, 11, and seven of Fig. 1 were energized. Measurements were observed and recorded. Then, the capacitor banks were de-energized one at a time until no capacitor banks were connected. After each capacitor bank was de-energized, measurements were taken and

recorded. The capacitor bank internal to the customer at node 25 of Fig. 1 was not de-energized for any of the configurations [4]. It is that set of six measurements that this study compares to *HARMFLO* simulations.

II. CURRENT DISTORTION

Power distribution systems are intended to provide a sinusoidal voltage of near constant magnitude for their connected loads. However, there are many types of non-linear loads connected to power distribution systems that draw currents which are not strictly sinusoidal at the frequency of the forcing function. Such loads effectively inject nonsinusoidal currents into the power distribution systems to which they are connected. These nonsinusoidal currents are a distortion to the system current flow, distort the system voltage, and may be periodic or aperiodic. [1],[3]

A. TRANSIENTS

Transients in the current flow of a power distribution system are aperiodic, discontinuous, and associated with events. These events are short in duration; the disturbances they cause in the system current flow typically decay within a few cycles of the system forcing function. The frequency content of transient disturbances is related to the natural modes of the system rather than the applied forcing function. [7] This study utilizes steady state analysis and does not address transients or their effects on power distribution systems.

B. HARMONICS

Any periodic signal satisfying the *Dirichlet conditions* can be represented by a sum of orthogonal basis functions. When the basis functions are sinusoids, a *Fourier Series* results. A signal represented by its *Fourier Series* is a sum of sinusoids at integer multiples of the fundamental frequency. [8] In power distribution systems, the fundamental is the frequency of the applied forcing function and periodic, non-sinusoidal currents injected by nonlinear loads are referred to as *harmonics* [1].

1. Harmonic Sources

There are a number of various devices that produce harmonic currents. Whereas all harmonic producing loads are not similar, most may be categorized as ferromagnetic devices, electronic power converters, or arcing devices. [3],[9:pp. 2–3]

a. Ferromagnetic devices

Motors and transformers are the most common power distribution system loads [9:pp. 2–3]. Both are essentially a coil of wire around an iron core and draw nonsinusoidal currents from the power distribution system. Transformers generate significant harmonic current levels because their cores normally saturate at the peak magnitude of the voltage source. Motors induce lower harmonic levels than transformers because their cores include high reluctance air gaps that do not saturate. Typical no-load transformer magnetizing current harmonic levels relative to the fundamental are shown in Table 1. [3]

TABLE 1: NO-LOAD TRANSFORMER CURRENT HARMONICS

Harmonic	Magnitude
3rd	50.0%
5th	20.0%
7th	5.0%
9th	2.6%

Transformer magnetizing currents are small compared to currents of other harmonic producing loads—typically 0.5% to 1.0% of rated load currents. Harmonic levels in magnetizing currents depend on voltage and loading levels. Additionally, currents with harmonic numbers that are multiples of three are referred to as *triplen* harmonics and cannot flow to delta connected transformers if the system to which they are connected is balanced. Therefore, triplen harmonics circulate through the windings

of delta connected transformers in balanced three phase systems rather than returning through the neutral conductor. [1],[9:pp. 1, 11],[10]

b. Electronic power converters

Although there are many types of electronic power converters in service, switch mode power supplies (SMPS) and line commutated devices are being used with increasing regularity [3]. Personal computers, copy machines, and a host of other electronic devices use switch mode power supplies because they offer reduced size and weight with increased efficiency and reliability compared to other types of power supplies. [11]

(1) Switch Mode Power Supplies. The most common harmonic producing single phase load is the SMPS. Figure 2 shows a typical SMPS configuration. [11]

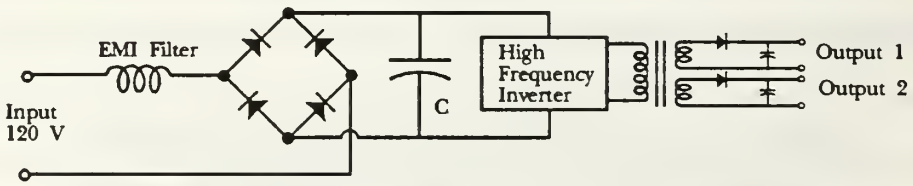

Fig. 2: A typical SMPS configuration

The diodes conduct when the input voltage exceeds the potential across the capacitor *C* in Fig. 2. Because conduction begins near the peak of the input voltage waveform, the current waveform is not sinusoidal and the power factor is low. The harmonic content of the input ac current waveform depends on the design of the SMPS, the applied load, and the value of *C*. Of these factors, *C* is the most important because the dc ripple and harmonic levels both depend on it. [11]

To illustrate this dependence, a typical SMPS configuration loaded with common electronic equipment is simulated with the *SPICE* program. The entries

listed in Table 2 depict the resulting RMS harmonic levels of the input ac current as a percentage of the fundamental. [11]

TABLE 2: SMPS CURRENT HARMONICS

Harmonic	C = 75 mF	C = 1000 mF
3rd	80%	95%
5th	50%	87%
7th	27%	74%
9th	21%	62%
11th	20%	48%
13th	15%	37%
15th	13%	27%
17th	12%	23%
THD	106%	178%

(2) Line Commutated Circuits. The basic configuration of a six pulse line commutated circuit is shown in Fig. 3. These circuits operate as rectifiers, inverters, or both. Rectifiers and inverters are essentially the same, except that the polarities of E and v_d are reversed. The current, i_d, flows the same direction for both; consequently, the direction of average power flow is opposite for rectifiers and inverters. Steady state operation in the inverter mode is possible only if there is a power source on the dc side. [12:pp. 51–52]

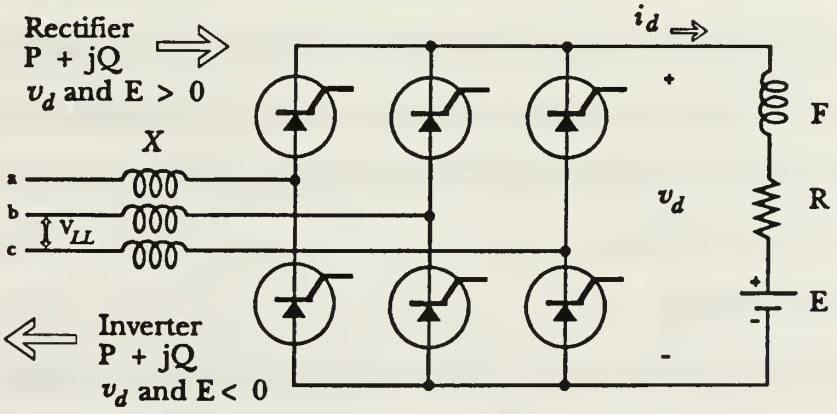

Fig. 3: A basic commutated rectifier/inverter circuit

The circuit of Fig. 3 is termed *line commutated* because there is no provision apart from the power distribution system to turn the thyristors off. The power distribution system effectively turns the thyristors off by negatively biasing them. The current commutates from one phase to the next when the negative bias is applied. [12:pp. 9–10, 587],[9:pp. 15–16],[6:pp. 20]

Many industrial applications such as dc motor drives use six pulse rectifiers. Two six pulse rectifiers can be connected together to form a twelve pulse rectifier. [13:pp. 2–1] Twelve pulse rectifiers generate significantly smaller fifth and seventh harmonic components in the ac line current than six pulse rectifiers. Table 3 lists typical harmonic levels in the ac line current as a percentage of the fundamental for six and 12 pulse rectifiers. [6:pp. 11–15, 22]

TABLE 3: TYPICAL RECTIFIER CURRENT HARMONICS

	Harmonic Number				
Type	5th	7th	11th	13th	17th
6 Pulse	17.5%	11.1%	4.5%	2.9%	1.5%
12 Pulse	2.6%	1.6%	4.5%	2.9%	2.0%

Unlike the SMPS of the previous section, the rectifier referred to here is a three phase circuit and does not produce triplen harmonics. Single phase rectifiers are used in some applications, primarily household appliances, and do produce triplen harmonics. Additionally, the harmonic levels depend on a host of parameters; six pulse rectifier parameters and their effect on harmonic current levels are discussed in Chapter IV. [3],[9:pp. 15–16]

c. Arcing Devices

Fluorescent lighting, arc welders, and arc furnaces are examples of arcing devices. Of these, arc furnaces cause the greatest harmonic disturbances because of their high power ratings. Arcing devices are essentially a voltage clamp in series with

a reactance connected to a single phase. Figure 4 shows a typical configuation of a circuit with an arcing device. [3],[9:pp. 15, 29]

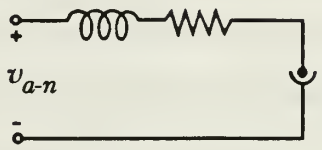

Fig. 4: A typical configuration of an arcing device circuit

The reactance limits current flow and is normally supplied by a transformer, ballast, or furnace leads. AC input current harmonic levels for typical single phase arcing devices are listed as a percentage of the fundamental in Table 4. [3], [9:pp. 15, 29]

TABLE 4: ARCING DEVICE HARMONICS

Harmonic	Magnitude
3rd	29.0%
5th	7.6%
7th	3.1%
9th	2.0%

C. EFFECTS OF CURRENT DISTORTION

Power distribution systems can normally absorb substantial levels of harmonic currents without significant difficulties. Harmonic currents generally flow from their nonlinear load sources toward the power source. If the generation source impedance is small compared to the system load impedances, voltage distortion will be low and most harmonic currents will find a return path through the system generators. The harmonic currents do, however, cause increased losses in power transformers and generators. Additionally, localized hot spots may develop and cause insulation failure. [1],[3], [9:pp. 44–46]

Most power distribution systems have capacitor banks installed at strategic locations to correct low power factors. These capacitor banks substantially change the nature of the system impedance. Instead of a low, purely inductive system impedance, the system impedance is mixed and the circuit will have one or more natural resonant frequencies creating low impedance resonant paths. If the resonant frequencies are near odd harmonic frequencies, harmonic currents may be diverted to the these low impedance resonant paths to neutral from their normal path through the system generators to neutral. [1],[3],[9:pp. 19, 26–28, 43–49]

System resonances may be series or parallel. Of the two, parallel resonances are more common and occur most frequently with the generation source and capacitor bank reactances. The combined parallel impedance at the resonant frequency is large and causes *voltage distortion* and increased harmonic current levels. Capacitor banks can fail from excessively high voltage and/or heat from increased current levels created by this phenomenon. [1],[3],[9:pp. 26–28, 43–49]

Series resonances occur when capacitor banks are installed near feeder ends or on transformer secondaries. In either case, the capacitor is near the end of the line and the resonant impedance is the capacitor bank in series with the inductance of the line or transformer windings. Series resonances divert harmonic currents through the resonant path. As a result, loads not normally submitted to harmonics will be exposed and remote capacitor banks may fail. [1],[3],[9:pp. 26–28, 43–49]

Voltage distortion is the primary problem associated with harmonics. Resistive loads absorb more power because of increased voltage levels. Voltage harmonics generate flux harmonics in motors which create losses and cause heating and vibrations. Additionally, circuit breakers trip unnecessarily and electronic equipment malfunctions. [1],[3],[9:pp. 43–49]

III. SOLVING THE POWER FLOW PROBLEM

A. THE FUNDAMENTAL LOAD FLOW

A power distribution system study based on the power flowing through the system is referred to as a *load flow* study. The active and reactive power load at each node and the self and mutual admittances of all the lines must be specified. These power and admittance inputs are used to solve for the node voltages throughout the system which are normally the quantities of interest. [5:pp. 193–196]

The specified power flow to a node n is related to the voltage and current at that node by the relation

$$P_n + jQ_n = V_n I_n^* \tag{3.1}$$

where $j = \sqrt{-1}$, P_n is the active power, Q_n is the reactive power, V_n is the voltage, and I_n is the current flow to node n [5:pp. 193–196]. The asterisk on I indicates complex conjugation. Solving for the current,

$$I_n = \frac{P_n - jQ_n}{V_n^*}. \tag{3.2}$$

Active power is absorbed when current flows through an admittance. Apparent power is conserved at each node. Applying Kirchhoff's current law at each node and Ohm's law between each node, the voltage at any node n in an N node system is

$$V_n = \frac{1}{Y_{nn}}\left(\frac{P_n - jQ_n}{V_n^*} - \sum_{k=1}^{N} Y_{nk} V_k\right) \tag{3.3}$$

where Y_{nn}, the self admittance at node n, is the sum of all admittances terminating on node n [5:pp. 170]. The mutual admittance, Y_{nk}, is the admittance between nodes n and k. The voltage magnitude and phase angle are normally specified at the system power

source called the swing bus. The swing bus is usually numbered one; therefore, V_n is calculated for values of n from two to N. [5:pp. 170, 193–196]

The system of $N-1$ nonlinear equations provided by equation (3.3) is of the form $\boldsymbol{Ax} = \boldsymbol{b}$ and is frequently solved iteratively using the method of successive displacements, or Gauss-Seidel method. The procedure involves making an initial guess at the voltage of nodes two through N. These voltage estimates are inserted on the right hand side of the equations in (3.3) and evaluated for the voltages on the left hand side. The voltage calculated becomes the updated estimate. When the change between successive updates at all the nodes decays to a specified tolerance, the estimate is assumed to be the solution. [14:pp. 474–481],[5:pp. 194–196]

If the matrix $\boldsymbol{A}$ is positive definite, convergence is guaranteed for any initial guess. The difference between successive updates at each node will decrease by a nearly constant factor, c. The number of iterations required for convergence for a tolerance ε is at least

$$m \geq \frac{\ln \varepsilon}{\ln c}. \tag{3.4}$$

This number m is normally prohibitively large. Consequently, the correction to each update is frequently scaled by some constant called an acceleration factor. The calculation of an appropriate acceleration factor is difficult in the best of circumstances and is normally found by trial and error. For power systems, an acceleration factor of 1.6 is frequently used [5:pp. 194–196]. [14:pp. 474–481]

Another common way to solve the load flow equations is with the Newton-Raphson method of rootfinding. It is also an iterative method that requires an initial estimate and is based on a Taylor series expansion of equation (3.3) in the polar form

$$P_n - jQ_n = \sum_{k=1}^{N} \left| V_n V_k Y_{nk} \right| e^{j(\Theta_{nk} + \delta_k - \delta_n)}. \tag{3.5}$$

The phase angle of Y_{nk} is Θ_{nk} and δ_i is the phase angle of the voltage at the ith node. [5:pp. 196–199]

Decomposing equation (3.5) into its real and imaginary parts, the power components P_n and Q_n are

$$P_n = \sum_{k=1}^{N} |V_n V_k Y_{nk}| \cos(\Theta_{nk} + \delta_k - \delta_n) \tag{3.6}$$

and

$$Q_n = -\sum_{k=1}^{N} |V_n V_k Y_{nk}| \sin(\Theta_{nk} + \delta_k - \delta_n). \tag{3.7}$$

Both P_n and Q_n are functions of the voltage magnitude $|V_n|$ and voltage phase angle δ_n. Let $|V_n^{(0)}|$ and $\delta_n^{(0)}$ be the initial guess at the solution. The Taylor series expansion of $P_n(|V_n|, \delta_n)$ for the first iteration is

$$P_n^{(0)} = \sum_{k=1}^{N} |V_n^{(0)} V_k^{(0)} Y_{nk}| \cos(\Theta_{nk} + \delta_k^{(0)} - \delta_n^{(0)}) + \Delta|V_n^{(0)}| \left.\frac{\partial P_n}{\partial |V_n|}\right|_{|V_n^{(0)}|} + \Delta\delta_n^{(0)} \left.\frac{\partial P_n}{\partial \delta_n}\right|_{\delta_n^{(0)}} + \cdots \tag{3.8}$$

where the partial derivatives are obtained by differentiating equation (3.6). Evaluating equation (3.6) with $|V_n^{(0)}|$ and $\delta_n^{(0)}$ and subtracting it from equation (3.8), the change in active power for the first iteration is

$$\Delta P_n^{(0)} = P_n^{(0)} - P_n^{(def)} = \Delta|V_n^{(0)}| \left.\frac{\partial P_n}{\partial |V_n|}\right|_{|V_n^{(0)}|} + \Delta\delta_n^{(0)} \left.\frac{\partial P_n}{\partial \delta_n}\right|_{\delta_n^{(0)}} + \cdots \tag{3.9}$$

where $P_n^{(def)}$ is the value of active power at node n that was specified when the problem was defined. Making the standard engineering approximation by neglecting terms of order two or more, the resulting system of $N-1$ equations for an arbitrary iteration i in matrix form is [5:pp. 196–199]

$$\begin{bmatrix} \Delta P_2^{(i)} \\ \Delta P_3^{(i)} \\ \vdots \\ \Delta P_N^{(i)} \end{bmatrix} = \begin{bmatrix} \frac{\partial P_2}{\partial \delta_2^{(i)}} & \frac{\partial P_2}{\partial \delta_3^{(i)}} & \cdots & \frac{\partial P_2}{\partial \delta_N^{(i)}} & \frac{\partial P_2}{\partial \left|V_2^{(i)}\right|} & \frac{\partial P_2}{\partial \left|V_3^{(i)}\right|} & \cdots & \frac{\partial P_2}{\partial \left|V_N^{(i)}\right|} \\ \frac{\partial P_3}{\partial \delta_2^{(i)}} & \ddots & & \frac{\partial P_3}{\partial \delta_N^{(i)}} & \frac{\partial P_3}{\partial \left|V_2^{(i)}\right|} & \ddots & & \frac{\partial P_3}{\partial \left|V_N^{(i)}\right|} \\ \vdots & & \ddots & \vdots & \vdots & & \ddots & \vdots \\ \frac{\partial P_N}{\partial \delta_2^{(i)}} & \frac{\partial P_N}{\partial \delta_3^{(i)}} & \cdots & \frac{\partial P_N}{\partial \delta_N^{(i)}} & \frac{\partial P_N}{\partial \left|V_2^{(i)}\right|} & \frac{\partial P_N}{\partial \left|V_3^{(i)}\right|} & \cdots & \frac{\partial P_N}{\partial \left|V_N^{(i)}\right|} \end{bmatrix} \begin{bmatrix} \Delta \delta_2^{(i)} \\ \Delta \delta_3^{(i)} \\ \vdots \\ \Delta \delta_N^{(i)} \\ \Delta V_2^{(i)} \\ \Delta V_3^{(i)} \\ \vdots \\ \Delta V_N^{(i)} \end{bmatrix} \tag{3.10}$$

where the $\frac{\partial P_n}{\partial x_k^{(i)}}$ notation indicates $\left.\frac{\partial P_n}{\partial x_k}\right|_{x_k^{(i)}}$.

A similar set of $N-1$ equations is obtained by expanding the reactive power equation (3.7) using the same procedure presented for the active power equation (3.6). The combined set of $2(N-1)$ equations in matrix form is

$$\begin{bmatrix} \Delta \mathbf{P}^{(i)} \\ \Delta \mathbf{Q}^{(i)} \end{bmatrix} = \underbrace{\begin{bmatrix} \frac{\partial \mathbf{P}^{(i)}}{\partial \delta^{(i)}} & \frac{\partial \mathbf{P}^{(i)}}{\partial \left|\mathbf{V}^{(i)}\right|} \\ \frac{\partial \mathbf{Q}^{(i)}}{\partial \delta^{(i)}} & \frac{\partial \mathbf{Q}^{(i)}}{\partial \left|\mathbf{V}^{(i)}\right|} \end{bmatrix}}_{2(N-1)\times 2(N-1)} \begin{bmatrix} \Delta \delta^{(i)} \\ \Delta \left|\mathbf{V}^{(i)}\right| \end{bmatrix} \tag{3.11}$$

where $\Delta \mathbf{P}^{(i)}$, $\Delta \delta^{(i)}$, and $\Delta \left|\mathbf{V}^{(i)}\right|$ are the $(N-1)\times 1$ column vectors of equation (3.10). The column vector $\Delta \mathbf{Q}^{(i)}$ is the reactive power equivalent to the active power column vector $\Delta \mathbf{P}^{(i)}$ and the $2(N-1)\times 2(N-1)$ matrix is the jacobian, $\mathbf{J}^{(i)}$. The top half of $\mathbf{J}^{(i)}$ is the matrix of equation (3.10) and the lower half is its reactive power counterpart. [5:pp. 199]

The initial guess, $\left|\mathbf{V}^{(0)}\right|$ and $\delta^{(0)}$, is used to evaluate equations (3.6) and (3.7) for $\mathbf{P}^{(0)}$ and $\mathbf{Q}^{(0)}$. The differences between these calculated values and the problem definition values are $\Delta \mathbf{P}^{(0)}$ and $\Delta \mathbf{Q}^{(0)}$. The partial derivatives of equations (3.6) and (3.7) are evaluated with $\left|\mathbf{V}^{(0)}\right|$ and $\delta^{(0)}$ to form $\mathbf{J}^{(0)}$. [5:pp. 196–200],[2:pp. 12]

The values obtained for $\Delta P^{(i)}$, $\Delta Q^{(i)}$, and $\mathbf{J}^{(i)}$ are used to solve equation (3.11) for $\Delta\delta^{(i)}$ and $\Delta\left|V^{(i)}\right|$ using an appropriate numerical method. Forward backward substitution is one common alternative to matrix inversion because it requires about one-third as many operations as inverting **J**. [14:pp. 92],[3:pp. 12]

The values computed for $\Delta\delta^{(i)}$ and $\Delta\left|V^{(i)}\right|$ are used to update the node voltages

$$\left|V^{(i+1)}\right| = \left|V^{(i)}\right| + \Delta\left|V^{(i)}\right| \tag{3.12}$$

and

$$\delta^{(i+1)} = \delta^{(i)} + \Delta\delta^{(i)}. \tag{3.13}$$

Updates are computed until ΔP and ΔQ decay to a specified tolerance or the maximum number of permissible iterations is reached. If the desired tolerance of ΔP and ΔQ is obtained, the final node voltages are the solution. [2:pp. 12],[5:pp. 196–200]

The Newton-Raphson method is simple in form and has great flexibility. Divided differences are sometimes used to avoid computing partial derivatives. The number of iterations for convergence depends on the initial guess. If the initial guess is far from the solution, the iterate may diverge. Conversely, when the iterate is sufficiently close to the actual solution, convergence is rapid. Each iteration requires at least $N^2 + N$ function evaluations for a system of N nonlinear equations making it a very computationally expensive method. For that reason, other methods such as Gauss-Seidel may be used to refine the initial guess before applying the Newton-Raphson method. [14:pp. 54-56, 92-95]

B. THE *HARMFLO* SOLUTION

1. Solution Method

The *HARMFLO* problem formulation differs from the fundamental load flow problem of the previous section because it includes harmonic generating loads.

Detailed load models for line commutated circuits and nonlinear resistors are included. The terminal voltages of the defined nonlinear loads are represented by their Fourier Series and are related to their input currents by these models. [2:pp. 12–34]

The nonlinear loads are treated like current sources connected to the power distribution system. The initial estimate of currents injected and terminal voltages for nonlinear loads are obtained from model data based on the specified loads. Because reactances are frequency dependent, the power distribution system has self and mutual admittance matrices for the fundamental and also for each harmonic frequency of the injected current. Although these admittance matrices only relate the currents at a given frequency to the voltage at that same frequency, the system voltage response to one harmonic frequency may be related to the current injected at a different frequency. Additionally, the voltage distortion caused by injected harmonic currents will affect the injected current making an iterative solution necessary. [2:pp. 12–34],[17:pp. 270–283]

The iterative Newton-Raphson method is reformulated to include harmonic frequencies. Additional equations are required to solve for the harmonic node voltages. The equations are based on Kirchhoff's current law and the conservation of apparent power where appropriate. Xia and Heydt develop the additional equations required to accommodate line commutated circuits in Refs. [15] and [16]. The *HARMFLO* formulation extends these equations to include nonlinear resistors and a variety of parameter combinations for line commutated circuits not included in the original development. [2:pp. 12–34]

Whereas detailed formulation of the equations is beyond the scope of this study, the general results are stated here for completeness. For an n node system with m nonlinear busses, the linear busses are numbered one through $m - 1$. The swing bus

is the linear bus numbered one. The nonlinear busses are numbered m through n. Non-triplen odd harmonics from five to L are considered. [2:pp. 11–16]

The active and reactive power balance is

$$[\Delta \mathbf{W}] = \left[\mathbf{J}^{(1)} \quad \mathbf{J}^{(5)} \quad \cdots \quad \mathbf{J}^{(L)}\right]\left[\Delta \mathbf{V}^{(1)} \quad \Delta \mathbf{V}^{(5)} \quad \cdots \quad \Delta \mathbf{V}^{(L)}\right]^{\mathrm{T}} \tag{3.14}$$

where $[\Delta \mathbf{W}] = \begin{bmatrix} \Delta \mathbf{P} \\ \cdots\cdots \\ \Delta \mathbf{Q} \end{bmatrix}$, $\left[\Delta \mathbf{V}^{(k)}\right] = \begin{bmatrix} \Delta \delta^{(k)} \\ \cdots\cdots\cdots \\ \Delta \left|\mathbf{V}^{(k)}\right| \end{bmatrix}$, and the superscript k indicates harmonic order. The fundamental jacobian, $\mathbf{J}^{(1)}$, is the same as the square matrix in equation (3.11). Partial derivatives of equations (3.6) and (3.7) evaluated with k^{th} harmonic frequency component values are used to build the harmonic jacobian $\mathbf{J}^{(k)}$. [2:pp. 11–16]

The nonlinear device models use two state variables, α and β. The change in state variables for an iteration is defined to be

$$[\Delta \Phi] = \left[\begin{array}{cccc|cccc} \Delta\alpha_m & \Delta\alpha_{m+1} & \cdots & \Delta\alpha_n & \Delta\beta_m & \Delta\beta_{m+1} & \cdots & \Delta\beta_n \end{array}\right]^{\mathrm{T}}. \tag{3.15}$$

The k^{th} harmonic current injected at node t has real and imaginary parts $g_{t,r}^{(k)}$ and $g_{t,i}^{(k)}$, respectively, where $m \le t \le n$. The partial derivatives of nonlinear device currents with respect to nonlinear device state variables at the k^{th} harmonic are [2:pp. 11–16]

$$\mathbf{H}^{(k)} = \operatorname{diag}\begin{bmatrix} \dfrac{\partial g_{t,r}^{(k)}}{\partial \alpha_t} & \dfrac{\partial g_{t,r}^{(k)}}{\partial \beta_t} \\ \dfrac{\partial g_{t,i}^{(k)}}{\partial \alpha_t} & \dfrac{\partial g_{t,i}^{(k)}}{\partial \beta_t} \end{bmatrix}. \tag{3.16}$$

The harmonic jacobian that relates the k^{th} and j^{th} harmonics is indicated by $\mathbf{YG}^{(k,j)}$ and is defined as

$$\mathbf{YG}^{(k,j)} = \begin{cases} \mathbf{Y}^{(k,k)} + \mathbf{G}^{(k,k)}, & k = j \\ \mathbf{G}^{(k,j)}, & k \neq j \end{cases} \tag{3.17}$$

where $\mathbf{Y}^{(k,k)}$ is a matrix containing partial derivatives of the k^{th} harmonic injection currents with respect to the k^{th} harmonic bus voltages derived from the system admittance matrix. The partial derivatives of the k^{th} harmonic device currents with respect to the j^{th} harmonic applied voltages are derived from the nonlinear device models and form the matrix

$$\mathbf{G}^{(k,j)} = \left[\begin{array}{c|c} \mathbf{O}_{2(m-1),2(m-1)} & \mathbf{O}_{2(m-1),2n} \\ \hline \mathbf{O}_{2n,2(m-1)} & \operatorname{diag}\left[\begin{array}{cc} \dfrac{\partial g_{t,r}^{(k)}}{V_t^{(j)}\partial\Theta_t^{(j)}} & \dfrac{\partial g_{t,r}^{(k)}}{\partial V_t^{(j)}} \\ \dfrac{\partial g_{t,i}^{(k)}}{V_t^{(j)}\partial\Theta_t^{(j)}} & \dfrac{\partial g_{t,i}^{(k)}}{\partial V_t^{(j)}} \end{array}\right] \end{array}\right] \tag{3.18}$$

where $V_t^{(k)}$ and $\Theta_t^{(k)}$ are the k^{th} harmonic voltage magnitude and phase angle at the t^{th} bus, $\mathbf{O}_{i,j}$ is an $i \times j$ matrix of zeros, and $m \le t \le n$. [2:pp. 11–16]

If h harmonics in addition to the fundamental are considered, the set of $2n(1 + h) + 3m$ nonlinear equations in matrix form is

$$\begin{bmatrix} \Delta\mathbf{W} \\ \Delta\mathbf{I}^{(1)} \\ \Delta\mathbf{I}^{(5)} \\ \vdots \\ \Delta\mathbf{I}^{(L)} \end{bmatrix} = \begin{bmatrix} \mathbf{J}^{(1)} & \mathbf{J}^{(5)} & \cdots & \mathbf{J}^{(L)} & \mathbf{0} \\ \mathbf{YG}^{(1,1)} & \mathbf{YG}^{(1,5)} & \cdots & \mathbf{YG}^{(1,L)} & \mathbf{H}^{(1)} \\ \mathbf{YG}^{(5,1)} & \mathbf{YG}^{(5,5)} & \ddots & \mathbf{YG}^{(5,L)} & \mathbf{H}^{(5)} \\ \vdots & \vdots & \cdots & \vdots & \vdots \\ \mathbf{YG}^{(L,1)} & \mathbf{YG}^{(L,5)} & \cdots & \mathbf{YG}^{(L,L)} & \mathbf{H}^{(L)} \end{bmatrix} \begin{bmatrix} \Delta\mathbf{V}^{(1)} \\ \Delta\mathbf{V}^{(5)} \\ \vdots \\ \Delta\mathbf{V}^{(L)} \\ \Delta\Phi \end{bmatrix}. \tag{3.19}$$

These equations are solved in much the same way as the fundamental load flow equations of the previous section are solved. An initial guess is made at the harmonic voltages and nonlinear device state variables. The power and currents are evaluated with the estimated values. Changes in voltages and state variables are computed from

equation (3.19). With each iteration, the voltage and state variable estimates are updated with the computed values until the change in power and currents decay to the specified tolerance. [2:pp. 11–16]

The solution speed and memory requirements depend heavily on the system because of the large number of sparsely populated matrices. Typical solution times for two system sizes are shown in Table 5 for three common machines.

TABLE 5: TYPICAL SOLUTION SPEED FOR THREE COMMON MACHINES

Size	Speed		
	CDC 6600	Cyber 205	VAX 11/780
69 bus, 7 harmonics	800 seconds	8 seconds	3200 seconds
21 bus, 7 harmonics	350 seconds	4 seconds	1400 seconds

A *HARMFLO* version is also available for the IBM PC. The PC version is pre-compiled, dimensioned for a 50 bus system, and requires 512 kilobytes of main memory and a math coprocessor. A 100 bus version can be compiled in about two hours and requires an estimated one megabytes of expanded memory. [3:pp. 3.1–3.3, 3.36–3.38]

2. Assumptions and Limitations

In addition to the 50 bus limit for the PC version, the *HARMFLO* problem formulation assumes a balanced bilateral three phase system and delta connected nonlinear devices. Consequently, single phase loads are not permitted and all even and triplen harmonics are excluded. [2:pp. 12–13]

Nonlinear loads may only be one of the defined types. A static transformer tap ratio or phase shift may be defined; however, tap or phase changing under load is not allowed. The frequency range is limited to 1860 Hz and the fundamental can only be 60 Hz. Additionally, if the apparent power is specified at a nonlinear bus instead of the reactive power, the reactive power is computed without any range limits. [13:pp. 3.1, A.1–A.7, 1.6]

IV. MODELING THE SYSTEM UNDER TEST

A. THE POWER SOURCE

A 69 kV substation bus draws power from a station bus. The substation bus potential is stepped down to 12.5 kV and distributes power to Audrain County. The Thevenin equivalent impedance at the Audrain 12.5 kV feeder is $0.94j$ per unit. This figure includes the short circuit impedance of the transmission system and the sub-transient synchronous reactance of the system generators. A one line drawing of the system power source is shown in Fig. 5. [4]

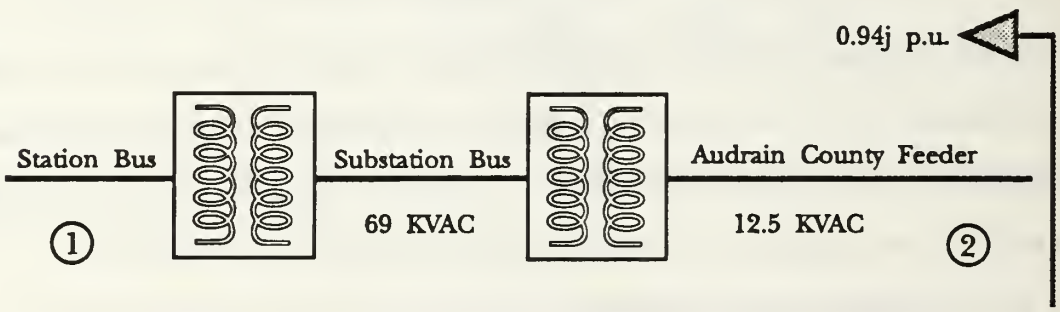

Fig. 5: A one line drawing of the system source

With *HARMFLO*, a system is driven by a source called a fundamental swing bus. The bus voltage is controlled to a percentage of the system voltage base. Only fundamental frequency currents are allowed on the swing bus. Once the source is specified, it may be connected to the rest of the system. [13:pp. 3.1–3.12]

Connections are specified by which nodes they connect and the equivalent impedance of the line expressed as a percentage of the system impedance base. This study does not address the *skin* or *long line* effects; however, *HARMFLO* does have hyperbolic long line and resistive skin effect models. These options are invoked by entering the base impedance and line length parameters. [13:pp. 3.14–3.18]

In addition to the normal paths, an option is provided for a *harmonics only* path. This option is necessary because harmonic currents will not have a path to ground through the swing bus. A path shunt to the swing bus with impedance equal to the short circuit impedance plus the subtransient synchronous reactance is required. The *HARMFLO* equivalent circuit model for the system source is shown in Fig. 6. [13:pp. 3.5–3.7]

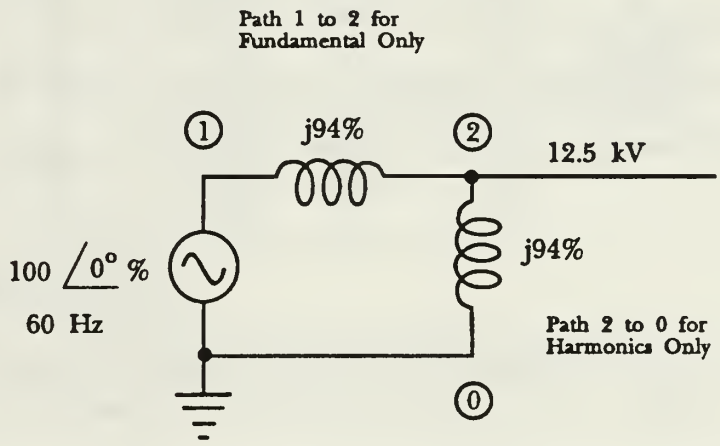

Fig. 6: The *HARMFLO* model of the system source

Note that the harmonic path to ground is connected to node zero. The connection between node zero and ground is implicit.

B. THE SOURCE OF HARMONICS

The dominant sources of harmonics in this system are the seven 100 HP adjustable speed dc drives shown lumped together at node 25 in Fig. 1. DC drives require ac to dc converters and rectifiers are the principle elements of such converters. Before simulating the entire Audrain subsystem, a circuit model of the dc drive and system source is simulated to determine the dc drive parameters. Parameters are adjusted until the desired response is obtained.

1. Modeling the Rectifier with *HARMFLO*

Six pulse rectifiers are used for this study because they are common to industrial applications such as dc motor drives. The *HARMFLO* circuit model of a six pulse rectifier is shown in Fig. 7. [13:pp. 2.1–2.4]

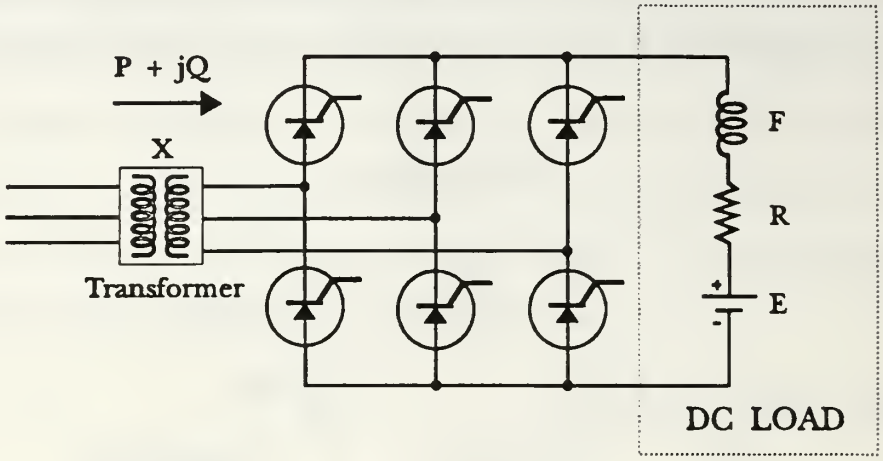

Fig. 7: The *HARMFLO* circuit model of a 6 pulse rectifier

Rectifiers may or may not have a dc source on the dc side of the circuit in Fig. 7. For dc drives, this source is equivalent to the back electromotive force voltage of the motor. If the dc source is chosen, *HARMFLO* will calculate the dc speed voltage E as one of the device state variables. If a rectifier without a dc source is chosen, $E = 0$. Frequently, a dc filter capacitor is used in shunt with the dc load. However, the effect on the harmonic content of the ac line current is small and the *HARMFLO* model does not include it. The parameters X, R, F, P, and Q identified in Fig. 7 must be specified as input parameters to *HARMFLO*. [13:pp. 2.1–2.4, B1–B10]

Rectifier transformers are modeled with *HARMFLO* by the equivalent reactance of the windings, X, expressed as a percentage of the system power base. The connection type such as Y–Y or Y–Δ must also be specified. Although the transformers are in three phase circuits and are not allowed to pass triplen harmonics with either connec-

tion type, the voltage phase angles differ by the standard 30° between Y and Δ connections. Additionally, if the resistance of the windings is significant, it may be lumped with the other components that make up the equivalent resistance, *R*. [13:pp. B1–B10]

For dc drives, *R* is comprised of the rectifier circuit and armature resistances. The reactance *F* represents the equivalent circuit reactance including filters and the dc machine reactance. Both are expressed as a percentage of the dc impedance base. The fundamental active and reactive power load of the drive are represented by *P* and *Q*, respectively. A permissible alternative is to specify the apparent and active power. In either case, the power quantities are expressed as a percentage of the system power base. [13:pp. 3.1–3.33]

2. DC Drive Parameters

The field study indicates that the customer operates the seven 100 HP adjustable speed dc drives on a one MVA base with a load of 500 kW and 309 kVAR [4]. Initially, one 700 HP adjustable speed dc drive is considered. One drive requires one six pulse rectifier for a dc voltage source. The rectifier parameters *R*, *F*, and *X* are unknown. Several assumptions are made to estimate these parameters for input to *HARMFLO*.

Assuming the rectifier transformer steps the 12.5 kV supplied by the utility down to 440 V and a commutation angle $\alpha = 0$, the average dc voltage is

$$V_d = \frac{3\sqrt{2}}{\pi} V_L \cos\alpha = \frac{3\sqrt{2}}{\pi}(440\ \text{V}) = 594.21\ \text{V}. \tag{4.1}$$

For a 700 HP load, the dc current is [12:pp. 46]

$$I_d = \frac{P}{V} = \frac{500\ \text{kW}}{594.21\ \text{V}} = 841.46\ \text{A}. \tag{4.2}$$

Assuming the converter has a dc filter choke with 5% losses, the loss due to the choke is

$$I^2R = 0.05 \times 500 \text{ kW} = 25 \text{ kW}. \tag{4.3}$$

Therefore, the choke has resistance

$$R = \frac{P_{loss}}{I_d^2} = \frac{25 \text{ kW}}{(841.46 \text{ A})^2} = 35.31 \text{ m}\Omega. \tag{4.4}$$

Since the type of wire in the choke is unknown, number 4/0 braided copper wire is assumed because of its current rating. Number 4/0 copper wire braided 19 by 0.106 inches has resistivity 0.049 ohms per thousand feet, a 0.528 inch copper diameter, and a 0.1662 square inch copper cross section. Polyurethane or polyvinylchloride insulation adds 550 pounds to every 1000 feet of wire for every cross sectional square inch of conductor. [18:pp. 277]

The density and cross sectional area of the insulation are

$$\rho_{ins} = \frac{\left(\frac{550 \text{ lbs}}{100 \text{ ft}}\right)}{\text{in}^2} \times 0.1662 \text{ in}^2 = 0.09141 \frac{\text{lbs}}{\text{ft}} \tag{4.5}$$

and

$$A_{ins} = \left(\frac{\rho_{ins}}{\rho_{cu}}\right) A_{cu} = \left(\frac{0.0914 \frac{\text{lbs}}{\text{ft}}}{0.6405 \frac{\text{lbs}}{\text{ft}}}\right) \times 0.1662 \text{ in}^2 = 0.0237 \text{ in}^2. \tag{4.6}$$

Therefore, a number 4/0 insulated wire has a diameter of about

$$d_{\#4/0} = 2\sqrt{\frac{A_{ins}}{\pi} + r_{cu}^2} = 2\sqrt{\left(\frac{0.024 \text{ in}^2}{\pi}\right) + \left(\frac{0.528 \text{ in}}{2}\right)^2} = 0.556 \text{ in}. \tag{4.7}$$

The choke has a total wire length of

$$W.L. = \frac{R}{\rho} = \frac{.03531\Omega}{\left(\frac{.049\Omega}{1000\text{ft}}\right)} = 720.61\text{ ft} = 219.63\text{ meters.} \tag{4.8}$$

Assuming a choke diameter of one meter, the circumference is 3.14 meters. With the assumed diameter, the choke has

$$N = \frac{W.L.}{\text{circumference}} = \frac{219.63}{\pi} = 70\text{ turns} \tag{4.9}$$

and a corresponding physical height of

$$h = (70)(0.556\text{ in})\left(\frac{.0254\text{ m}}{\text{in}}\right) = 0.99\text{ meters.} \tag{4.10}$$

The inductance of an air core solenoid choke is

$$L = \frac{\mu_0 N^2 A}{h}. \tag{4.11}$$

This expression can be manipulated to be

$$L = \frac{\mu_0 N^2 (\pi r^2)}{Nd} = \frac{\mu_0 \left(\frac{W.L.}{2\pi r}\right)(\pi r^2)}{d} = \frac{\mu_0 (W.L.) r}{2d} \tag{4.12}$$

where r is the radius of the solenoid and d is the diameter of the wire.[19:pp. 268] Numerically, the choke has inductance

$$L = \frac{\mu_0 (W.L.) r}{2d_{wire}} = \frac{\left(4\pi \times 10^{-7}\frac{\text{H}}{\text{m}}\right)(219.63\text{ m})(0.5\text{m})}{2(0.556\text{ in})\left(.0254\frac{\text{m}}{\text{in}}\right)} = 4.9\text{ mH.} \tag{4.13}$$

The dimensions and inductance are reasonable for an air core solenoid choke used to filter the converter of a 700 HP dc drive. Figure 8 illustrates the assumed dimensions of the choke and the wire used to construct it.

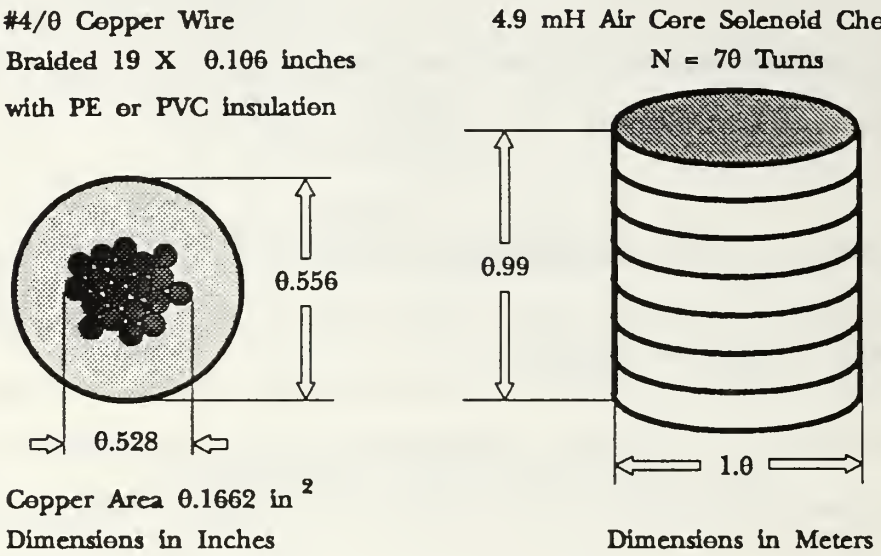

Fig. 8: Wire and choke dimensions

The motor base impedance is

$$Z_{motor} \cong \frac{V^2}{S} = \frac{(440\ \mathrm{V})^2}{588\ \mathrm{kVA}} = 329.3\ \mathrm{m\Omega}. \tag{4.14}$$

Assuming the armature resistance of the dc drive is 5% of the motor base impedance, the armature resistance is

$$R_A \cong 0.05 \times 329.3\ \mathrm{m\Omega} = 16.5\ \mathrm{m\Omega}. \tag{4.15}$$

The forward drop resistance of the rectifier SCR thyristors is neglected; therefore, the total resistance on the dc side of the circuit in Fig. 7 is

$$R_{Total} \cong R_{choke} + R_A = 35.3\ \mathrm{m\Omega} + 16.5\ \mathrm{m\Omega} = 52\ \mathrm{m\Omega}. \tag{4.16}$$

To convert the rectifier parameters for input to *HARMFLO*, the rectifier transformer secondary is assumed to be 440 V. The base dc voltage is

$$V_{BDC} = V_{BAC(l-n)} = \frac{440\text{ V}}{\sqrt{3}} = 254.03\text{ V}. \tag{4.17}$$

For consistency, the dc impedance base is defined to be the same as the ac impedance base and is given by

$$Z_{BDC} = Z_{BAC} = \frac{3V_{BAC(l-n)}^2}{S_B} = \frac{3(254.03\text{ V})^2}{10^6\text{ VA}} = 193.6\text{ m}\Omega. \tag{4.18}$$

Note that the appropriate power base is the one MVA power base which the customer operates on and not the 100 MVA system power base. [13:pp. B6–B9]

The equivalent resistance, R, is

$$R_{pu} = \frac{R_{Total}}{Z_{BDC}} = \frac{52\text{ m}\Omega}{193.6\text{ m}\Omega} = 0.2686\text{ pu}. \tag{4.19}$$

This per unit value must be further converted to the percentage

$$R_{\%} = 100 \times R_{pu} = 26.86\%. \tag{4.20}$$

The motor reactance is small relative to the choke and is neglected. Consequently, the total reactance in the dc circuit is [13:pp. B6–B9]

$$X_F = 120\pi L = 120\pi(4.9\text{ mH}) = 1.84\ \Omega, \tag{4.21}$$

and

$$F = \frac{X_F}{Z_{BDC}} = \frac{1.84\ \Omega}{0.1936\ \Omega} \times 100 = 951.62\ \%. \tag{4.22}$$

The rectifier transformer reactance is assumed to be 10% of the customer's impedance base. Several combinations of Y and Δ connections are evaluated for model performance. The transformer reactance expressed as a percentage of the system base is

$$X_{\%} = \frac{0.1\times10^{6}}{100\times10^{6}}\times100\% = 0.10\ \%. \tag{4.23}$$

The given rectifier load must be converted to a percentage of the system power base. The active power load is

$$P_{\%} = \frac{500\ \text{KW}}{100\ \text{MVA}}\times100 = 0.50\ \%. \tag{4.24}$$

The reactive power load obtained using the power triangle is

$$Q_{\%} = \frac{\sqrt{S^2 - P^2}}{S_B}\times100 = \frac{\sqrt{588{,}000^2 - 500{,}000^2}}{100\times10^{6}}\times100 = 0.31\ \%. \tag{4.25}$$

With these source and rectifier parameters, the minimal circuit model of Fig. 9 is input to *HARMFLO* and simulated. Model parameters are then varied and model performance assessed.

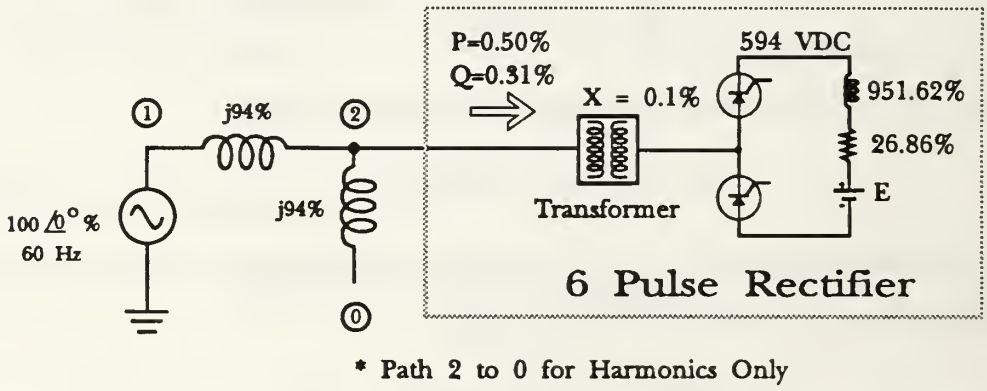

Fig. 9: Minimal single phase circuit model

3. Rectifier Model Performance

a. Theoretical Behavior

The rectifier will generate harmonics in the ac line current depending on the delay angle, α, and the commutating reactance, X [6:pp. 22]. The line current drawn by a six pulse rectifier is typically a quasi square wave. Figure 10 shows the theoreti-

cal line current for a six pulse rectifier with a Y–Y transformer connection. [12:pp. 57–59]

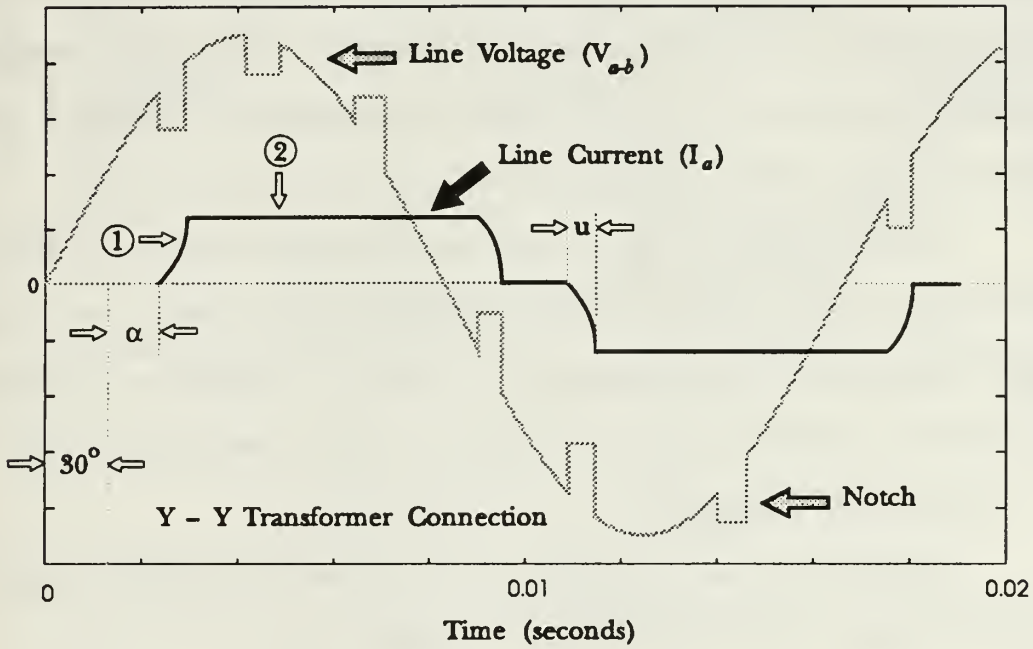

Fig. 10: Theoretical six pulse rectifier ac line current

The line and phase voltages of a Y–Y connected load are in step. Thirty degrees separates the negative to positive zero crossing of a sinusoidal phase voltage from the crossover point with an adjacent phase voltage. The angle at which the start of the quasi square wave exceeds this 30^{o} is defined as the delay angle, α. [12:pp. 55–60] Whereas the commutating reactance, X, must be specified by the user, α is normally computed by *HARMFLO* as one of the nonlinear device state variables. However, the delay angle may be specified as an input if it is known. [13:pp. 3.28–3.33]

The rising and falling edges of the quasi square wave indicated by bullet one in Fig. 10 are a function of the rectifier transformer reactance, X. If $X = 0$, the slope of the rising and falling edges is infinite and the commutation interval is zero. If

X is non-zero, the commutation interval, u, is non-zero. The commutation interval is also referred to as the commutating angle, μ. A non-zero commutating angle produces an observable *notch* in the line voltage because two adjacent phase voltages are shorted together through an SCR and the commutating reactance of the rectifier transformer during each time interval u. For this reason, the commutation interval, u, is also known as the notch width for the line voltage. [12:pp. 55–60],[6:pp. 11–15]

The flat surfaces of the quasi square wave indicated by bullet two in Fig. 10 are a function of the dc reactance, F. If F is infinite, the flat surfaces have no ripple. For finite values of F, the ripple depends on the value of F. The value of R determines which values of F satisfy the convergence criterion. [12:pp. 55–60],[6:pp. 11–15]

b. Actual Performance

Rectifier line current components are obtained from *HARMFLO* output for the circuit of Fig. 9. A time domain signal of the form

$$i(t) = \sum_{n=1}^{13} M_n \sin(120\pi nt + \phi_n) \tag{4.26}$$

is constructed where M_n is the magnitude and ϕ_n is the phase of the n^{th} harmonic current. The harmonic number n is considered for the values n = 1, 5, 7, 11, and 13. Simulated rectifier line currents for the circuit of Fig. 9 are shown in Fig. 11.

Model performance is identical for Y–Y and Δ–Δ connected rectifier transformers. It is also the same for Y–Δ and Δ–Y connections. Additionally, the mixed transformer connection models all produce identical magnitudes and phase angles to the like connection models with two exceptions. The phase angles of the 5^{th} and 7^{th} harmonics are shifted by 180°. This difference is the result of the 30° phase shift between phase voltages of Y and Δ connected transformers. Magnitudes of the current harmonics relative to the fundamental are listed in Table 6.

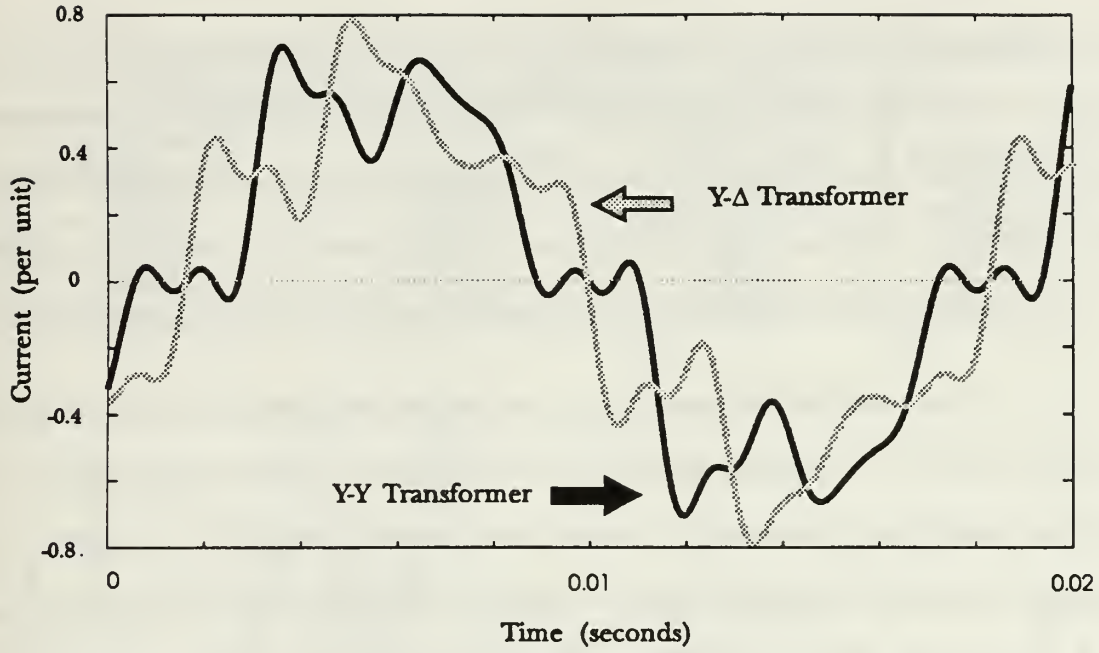

(a) Rectifier without a dc source

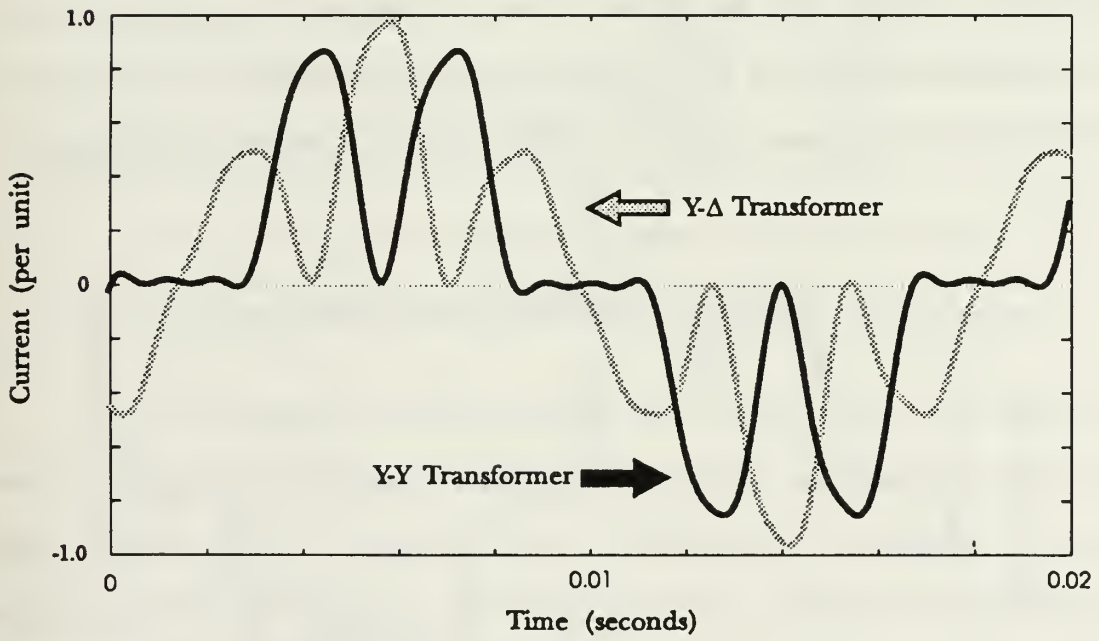

(b) Rectifier with a dc source

Fig. 11: Simulated rectifier line current for circuit of Fig. 9

TABLE 6: SIMULATED HARMONIC LINE CURRENT MAGNITUDES FOR THE CIRCUIT OF FIG. 9 (RELATIVE TO THE FUNDAMENTAL)

Harmonic #	Rectifier with a dc source	Rectifier without a dc source	Typical values from Table 3
5th	56.6%	28.4%	17.5%
7th	27.6%	11.9%	11.1%
11th	7.4%	11.3%	4.5%
13th	8.4%	5.7%	2.9%

The simulated values of Table 6 are considerably different than the typical values of Table 3. To isolate the cause, each parameter is varied independently. The rectifier transformer reactance X is varied over a range from 0.01% to 1000%. The simulated results for the model with a dc source more closely match the typical values as X is increased. With X = 100%, the fifth harmonic is only 4.4% smaller relative to the fundamental, whereas at 1000%, it is 23.2% less. The model without a dc source shows little variation as the transformer reactance is changed. The fifth harmonic current magnitude changes only 1.4% relative to the fundamental over the full range of X. Figure 12 shows the extreme case of X = 1000% with Y–Y connected transformers.

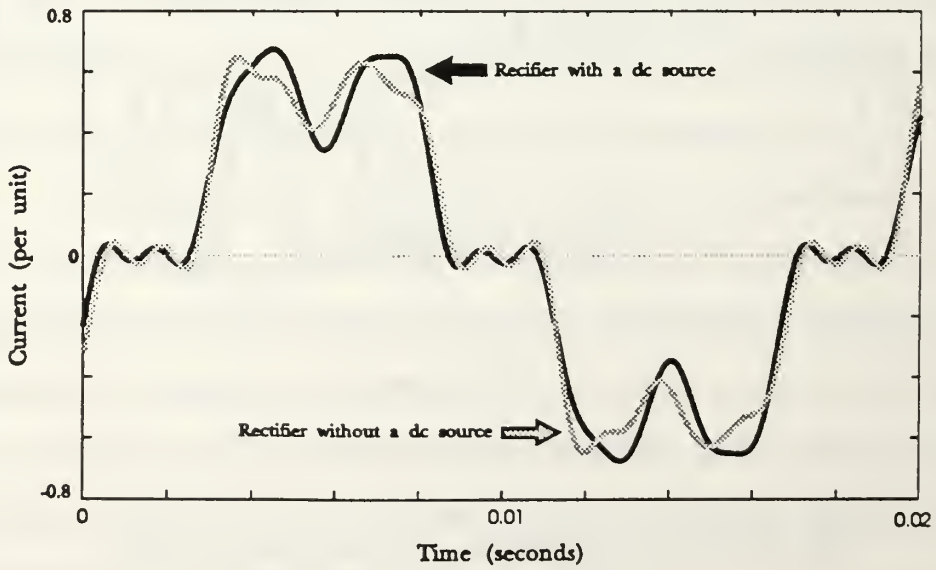

Fig. 12: Simulated rectifier line current with extreme transformer reactance

The dc circuit reactance, F, is varied over a wide range. The rectifier line current for the model without a dc source does not change; however, the line current for the model with a dc source has less ripple when F is increased. The *HARMFLO* solution converges for values of F between 100% and 1350% with R = 26.86%. Figure 13 illustrates how the line current changes for the model with a dc source.

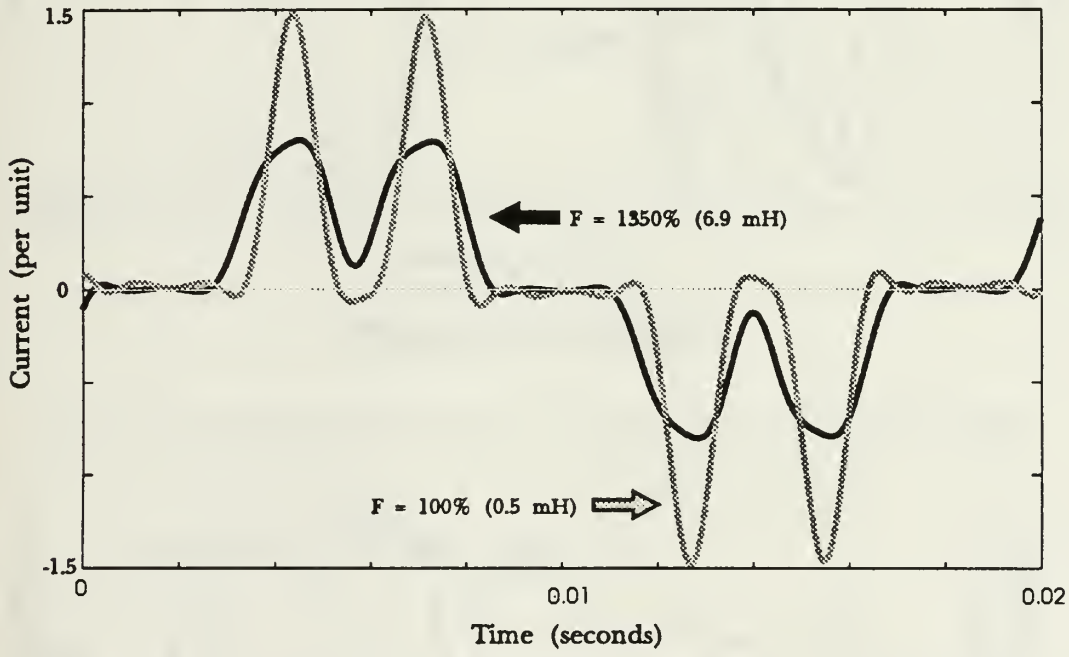

Fig. 13: Simulated rectifier line current as a function of dc circuit reactance

The equivalent dc circuit resistance, R, is varied over a wide range and makes no significant difference in the line current for the rectifier model with a dc source. For the model without a dc source, R is calculated by *HARMFLO* from the voltage and active power at the rectifier bus. The active power load level affects the line current as illustrated in Fig. 14.

The power factor also affects the rectifier line current. Figure 15 shows how the line current changes in response to a varying power factor.

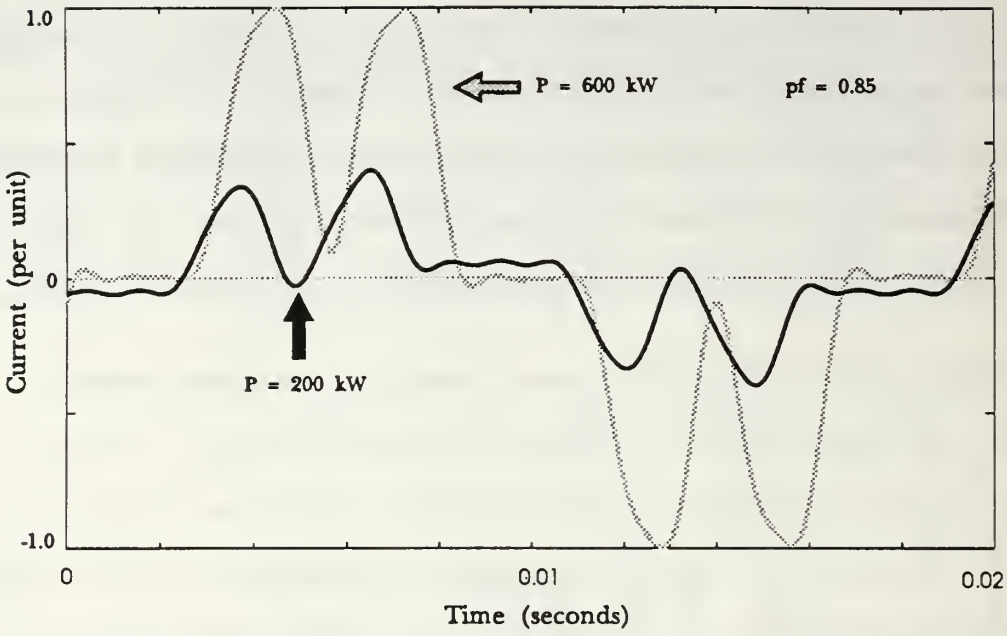

(a) Rectifier with a dc source

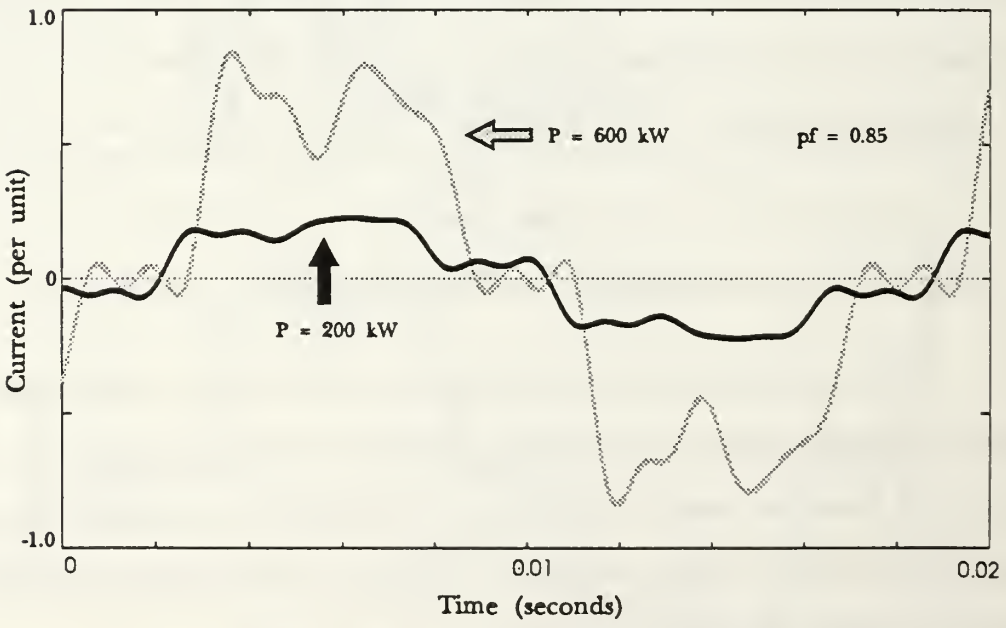

(b) Rectifier without a dc source

Fig. 14: Rectifier line current as a function of active power load

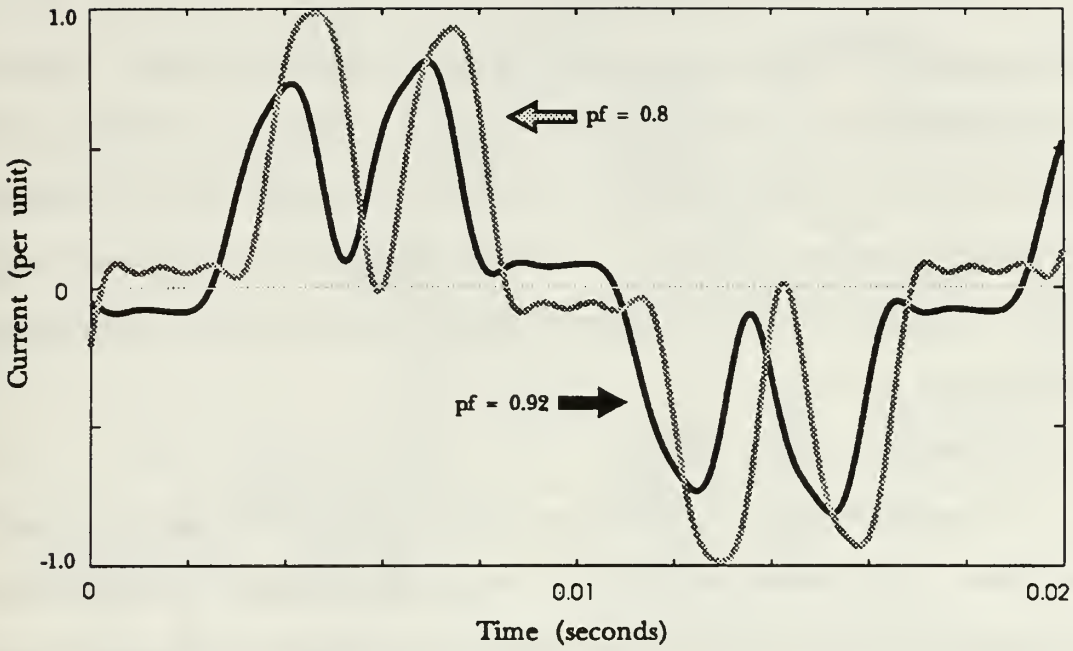

(a) Rectifier with a dc source

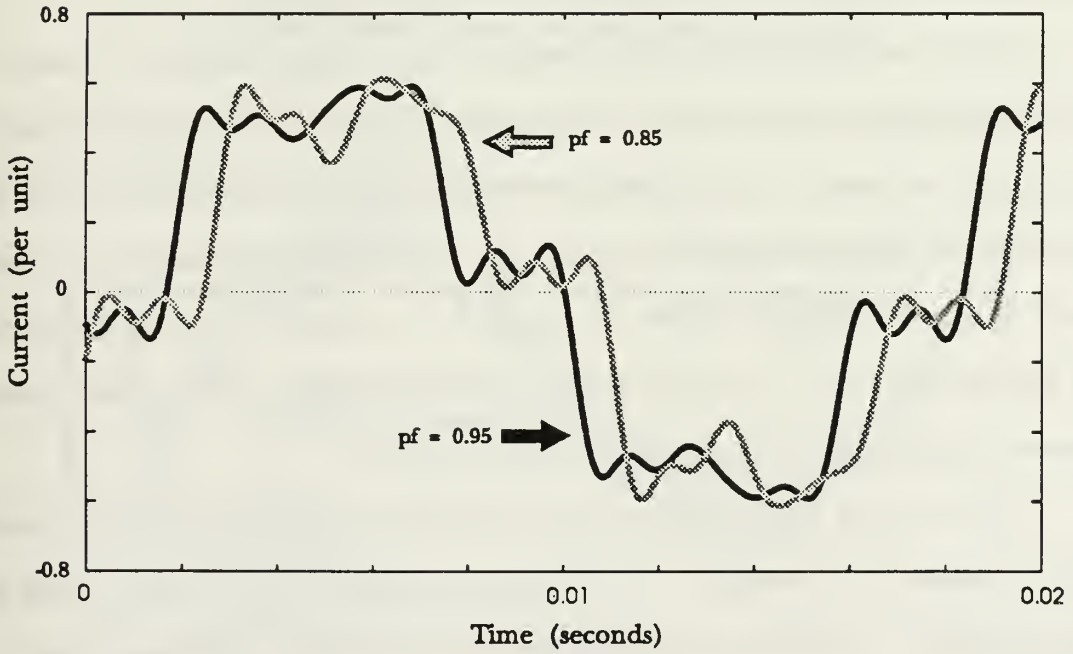

(b) Rectifier without a dc source

Fig. 15: Rectifier line current as a function of power factor

The model that best approximates the quasi square wave of Fig. 10 is the rectifier with a Y–Y or Δ–Δ transformer connection without a dc source. Simulation results indicate that the estimated parameter values are reasonable. However, the fifth harmonic of the line current is significantly larger than typical values. Furthermore, the customer operates seven drives. It is likely that the drives are operated independently. Therefore, modeling the drives by lumping them all together is an inadequate approximation.

4. A Revised Rectifier Model

For a system with multiple nonlinear loads, harmonic levels may be reduced by cancellation. This cancellation is achieved by alternating between Y–Y and Y–Δ rectifier transformer connections at adjacent loads. If the loads are split evenly between Y–Y and Y–Δ connected converters, a 12 pulse rectifier results and the fifth and seventh harmonic line currents are significantly reduced. [13:pp. 2.8]

The seven 100 HP adjustable speed dc drives are split between Y–Y and Y–Δ connected rectifiers. However, there are an odd number of drives making it impossible to split the load evenly. Assuming the customer powers four of the drives with Y–Δ connected rectifiers and three drives with Y–Y connected rectifiers and that the load is evenly distributed among all seven drives, a 57% Y–Δ to 43% Y–Y load split results. The parameters X, R, F, P, and Q are all scaled accordingly. The revised minimal equivalent single phase circuit model is shown in Fig. 16.

The circuit of Fig. 16 is simulated for rectifiers with and without a dc source. AC line currents are generated with components obtained from *HARMFLO* output and equation (4.26). The resulting waveforms are shown in Fig. 17. Harmonic levels expressed as a percentage of the fundamental are listed in Table 7.

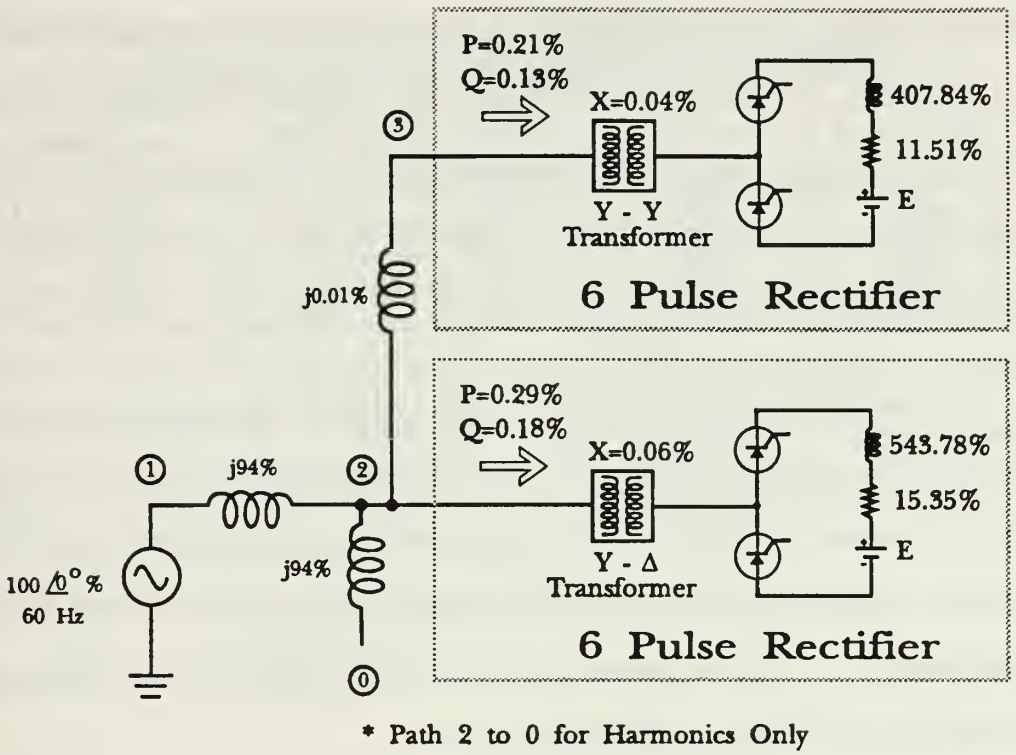

Fig. 16: Revised minimal single phase circuit model

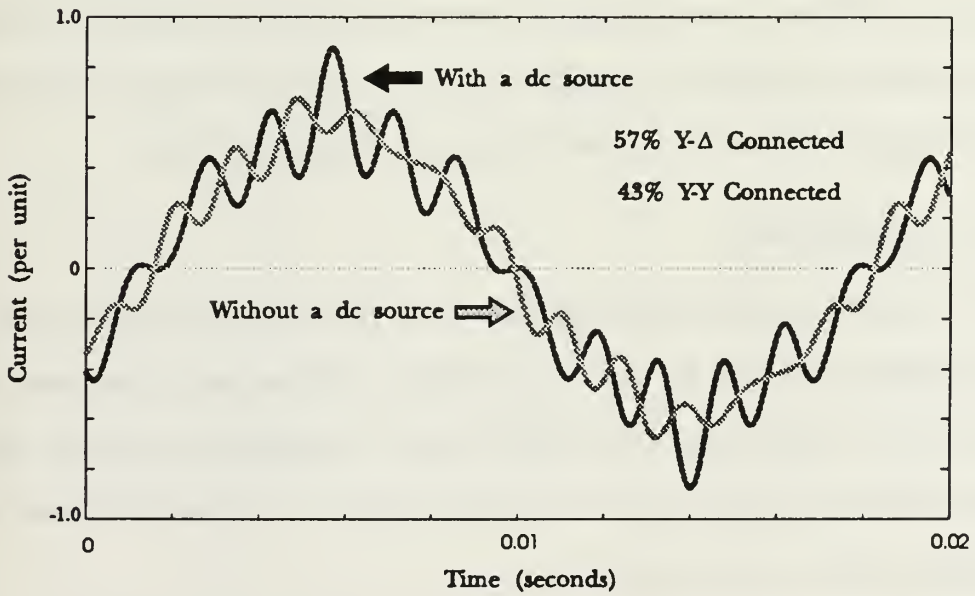

Fig. 17: Simulated rectifier line current for the circuit of Fig. 16

TABLE 7: SIMULATED HARMONIC LINE CURRENT MAGNITUDES FOR THE CIRCUIT OF FIG. 16(RELATIVE TO THE FUNDAMENTAL)

Harmonic #	Rectifier with a dc source	Rectifier without a dc source	Typical 6 pulse values from Table 3	Typical 12 pulse values from Table 3
5th	9.2%	4.6%	17.5%	2.6%
7th	3.9%	2.0%	11.1%	1.6%
11th	25.2%	11.5%	4.5%	4.5%
13th	10.1%	7.1%	2.9%	2.9%

The simulated current waveforms shown in Fig. 17 are similar to idealized 12 pulse rectifier line currents [12:pp. 387–389]. The simulated harmonic levels listed in Table 7 fall between the typical values for six and 12 pulse rectifiers from Table 3. The model is significantly less accurate at frequencies above the seventh harmonic. This inaccuracy is of little consequence for this study because field measurements were not recorded for harmonic orders larger than seven.

The rectifier with a dc source is selected because it more closely resembles the physical circuit being modeled and also because of its fifth harmonic line current magnitude. At 9.2%, it is roughly half of the typical six pulse value listed in Table 3. A realistic goal when alternating rectifier transformer connection types might be to reduce the largest single harmonic current magnitude by a factor of two.

C. LOAD MODELING

The computer analysis uses the estimated load values from the field study. The general procedure is stated here for completeness. The customer's nonlinear load is based on a 700 HP load with a 0.85 power factor. The difference between the total measured voltampere load at node 25 and the customer's estimated nonlinear load is the linear load estimate at node 25. [4]

To estimate the other loads, each feeder is considered separately. The ratio of the total measured apparent power to the sum of all the connected transformer ratings is

computed for each feeder. This ratio scales the transformer ratings and produces an estimate of the loads connected to that feeder. For feeder 53, the scale factor is computed without the customer's load because the load at node 25 is already estimated. [4]

Several nodes in Fig. 1 represent more than one transformer. Although there are some residential loads on feeder 51, feeder 52 is predominantly residential loads. A number of the nodes on feeders 51 and 52 represent small residential areas with more than one house connected. Whereas each house normally has its own transformer, the system grows arbitrarily large if the nodes are not grouped in this manner. [4]

V. SIMULATION RESULTS

The system of Fig. 1 is simulated using the revised rectifier model to approximate the customer's seven 100 HP adjustable speed dc drives. Six system impedance configurations are simulated. These configurations facilitate evaluation of nonlinear load modeling accuracy and prediction accuracy of system-wide harmonic propagation. Table 8 lists the six system configurations.

TABLE 8: SIMULATION IMPEDANCE CONFIGURATIONS

	Run 1	Run 2	Run 3	Run 4	Run 5	Run 6
Capacitors Connected at Nodes	7	7	7	7	7	—
	11	11	11	11	—	—
	16	16	16	—	—	—
	19	19	—	—	—	—
	24	—	—	—	—	—
	25	25	25	25	25	25

The accuracy of the simulated current at node 24 is a measure of the nonlinear load model effectiveness. Table 9 lists the simulation results and field measurements of I_{24}.

TABLE 9: CURRENT AT NODE 24—FIELD DATA AND SIMULATION RESULTS

Run	**Fundamental (Amperes)**		**Fifth (% of Fund.)**		**Seventh (% of Fund.)**		**THD (% of Fund.)**	
	Field Data	Simulation	Field Data	Simulation	Field Data	Simulation	Field Data	Simulation
1	67.71	54.50	6.55	6.25	1.30	1.87	6.68	6.51
2	68.92	55.43	6.23	5.93	1.34	1.66	6.38	6.18
3	67.39	55.89	6.51	5.59	1.30	2.43	6.67	6.11
4	68.92	55.89	6.37	5.45	1.14	2.65	6.49	6.04
5	61.43	56.35	8.05	5.33	2.56	2.64	8.45	5.96
6	67.39	56.81	6.10	5.18	2.33	2.50	6.49	5.77

The simulated current fundamentals are consistently smaller than the measured values. However, the simulated harmonic current to fundamental current ratios are similar to

the measured ratios. Figure 18 illustrates how the simulated and measured values change in response to a varying system impedance.

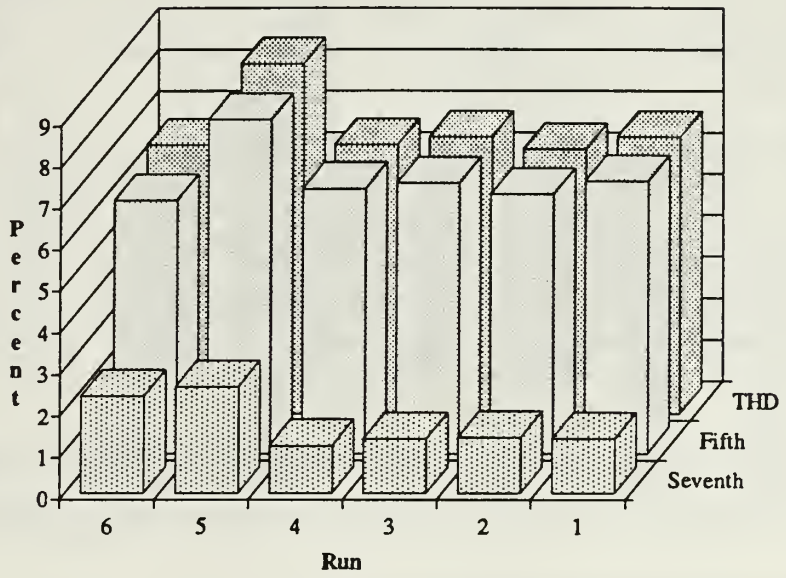

(a) Field measurements

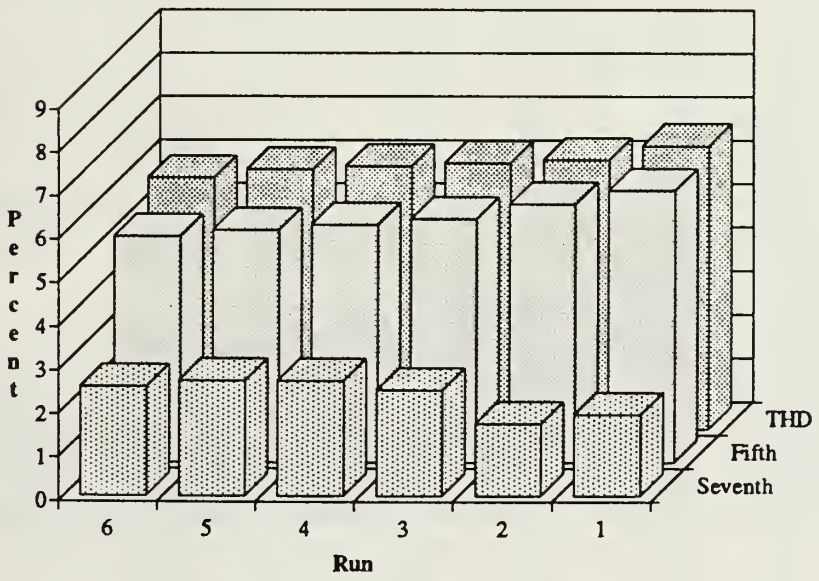

(b) Simulated values

Fig 18: Node 24 current harmonics and THD relative to the fundamental

The simulated and measured voltage quantities at node 24 are similar. Table 10 summarizes the simulated and measured values.

TABLE 10: VOLTAGE AT NODE 24—FIELD DATA AND SIMULATION RESULTS

Run	Fundamental (kV)		Fifth (% of Fund.)		Seventh (% of Fund.)		THD (% of Fund.)	
	Field Data	Simulation	Field Data	Simulation	Field Data	Simulation	Field Data	Simulation
1	12.40	12.57	0.96	1.60	0.60	0.34	1.13	1.64
2	12.30	12.45	0.34	0.97	0.90	0.58	0.97	1.13
3	12.20	12.34	0.38	0.67	0.83	0.74	0.91	1.00
4	12.30	12.29	0.31	0.59	0.75	0.61	0.81	0.85
5	12.30	12.25	0.32	0.55	0.37	0.51	0.49	0.75
6	12.30	12.18	0.33	0.48	0.27	0.32	0.43	0.58

Unlike the current fundamentals at node 24, the simulated voltage fundamentals are not significantly different than the measured values. Figure 19 illustrates the differences in simulated and measured voltage THD.

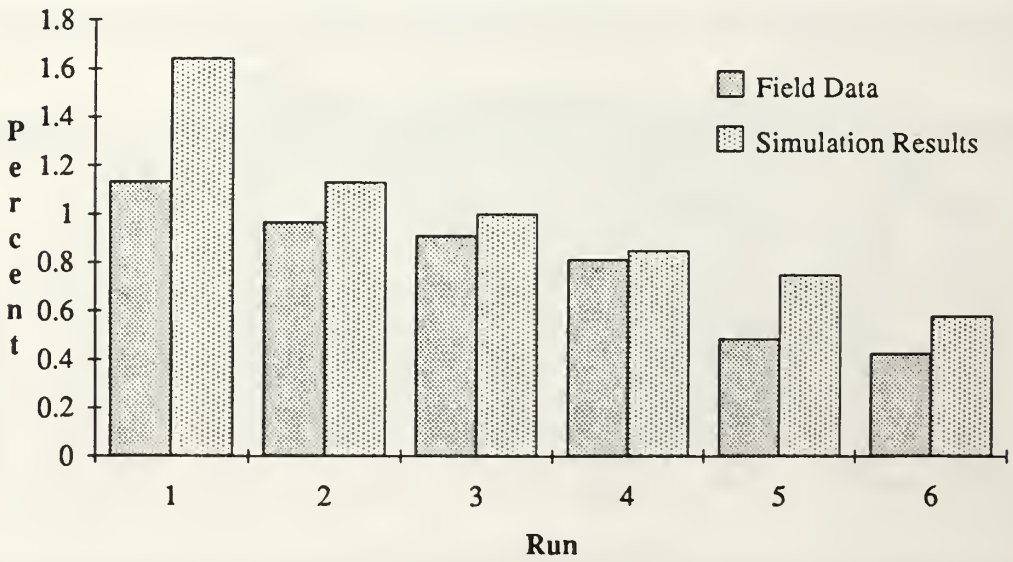

Fig. 19: Simulated and measured voltage THD at node 24

Comparisons of the simulated feeder currents to field measurements indicate how closely the system model approximates the actual system and how well *HARMFLO* predicts propagation of the injected harmonic currents. Tables 11, 12, and 13 summarize the simulated and measured current values for feeders 51 through 53.

TABLE 11: FEEDER 51 CURRENT($I_{2\text{-}11}$)—FIELD DATA AND SIMULATION RESULTS

Run	Fundamental (Amperes)		Fifth (% of Fund.)		Seventh (% of Fund.)		THD (% of Fund.)	
	Field Data	Simulation	Field Data	Simulation	Field Data	Simulation	Field Data	Simulation
1	23.74	24.94	1.36	3.30	1.17	1.18	1.86	3.51
2	25.54	24.94	1.45	1.97	2.17	2.00	2.54	2.81
3	26.37	24.94	1.40	1.35	2.45	2.52	2.82	2.84
4	26.37	25.40	1.58	1.15	1.93	1.97	2.50	2.30
5	29.79	27.71	1.09	0.33	0.31	0.35	1.20	0.48
6	31.13	27.71	0.19	0.26	0.30	0.18	1.20	0.32

TABLE 12: FEEDER 52 CURRENT($I_{2\text{-}3}$)—FIELD DATA AND SIMULATION RESULTS

Run	Fundamental (Amperes)		Fifth (% of Fund.)		Seventh (% of Fund.)		THD (% of Fund.)	
	Field Data	Simulation	Field Data	Simulation	Field Data	Simulation	Field Data	Simulation
1	26.82	28.64	4.92	7.30	6.15	3.86	8.70	8.31
2	26.37	28.64	3.68	4.37	13.66	6.56	13.00	7.95
3	26.37	28.18	3.15	3.04	16.11	8.38	14.00	8.85
4	25.54	28.18	3.07	2.63	14.10	6.68	13.50	7.12
5	25.54	28.18	2.17	2.37	9.40	5.22	9.30	5.69
6	26.37	26.79	2.45	0.26	1.05	0.17	3.50	0.31

TABLE 13: FEEDER 53 CURRENT($I_{2\text{-}15}$)—FIELD DATA AND SIMULATION RESULTS

Run	Fundamental (Amperes)		Fifth (% of Fund.)		Seventh (% of Fund.)		THD (% of Fund.)	
	Field Data	Simulation	Field Data	Simulation	Field Data	Simulation	Field Data	Simulation
1	134.97	109.93	5.20	7.64	1.47	0.70	6.40	7.66
2	143.74	108.08	3.34	4.65	1.29	1.21	4.50	4.81
3	146.15	113.63	3.38	3.03	0.60	1.44	4.30	3.36
4	79.86	118.71	2.89	2.50	1.04	1.10	3.80	2.73
5	151.73	119.17	2.83	2.47	1.00	1.15	3.80	2.72
6	151.73	120.09	2.59	2.41	0.97	1.16	3.50	2.68

Figure 20 shows how the simulated and measured THD values compare for the three feeders.

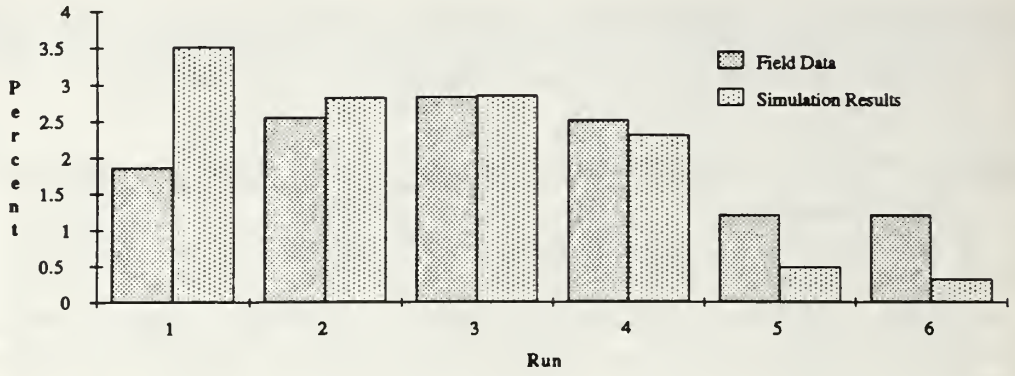

(a) Feeder 51

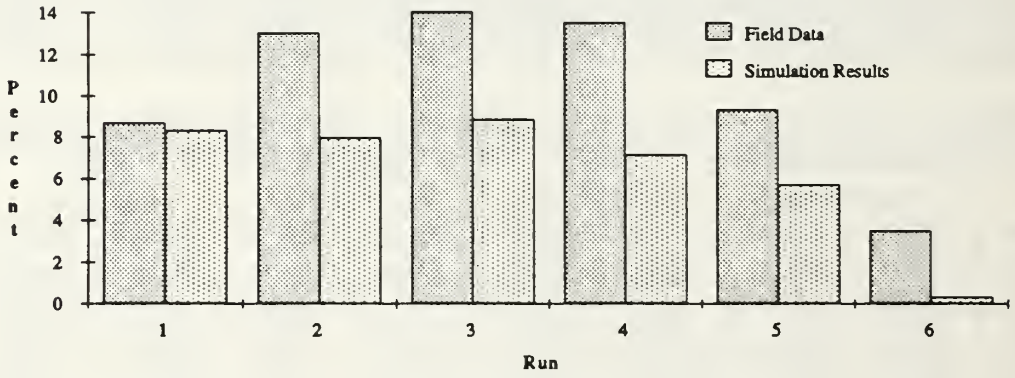

(b) Feeder 52

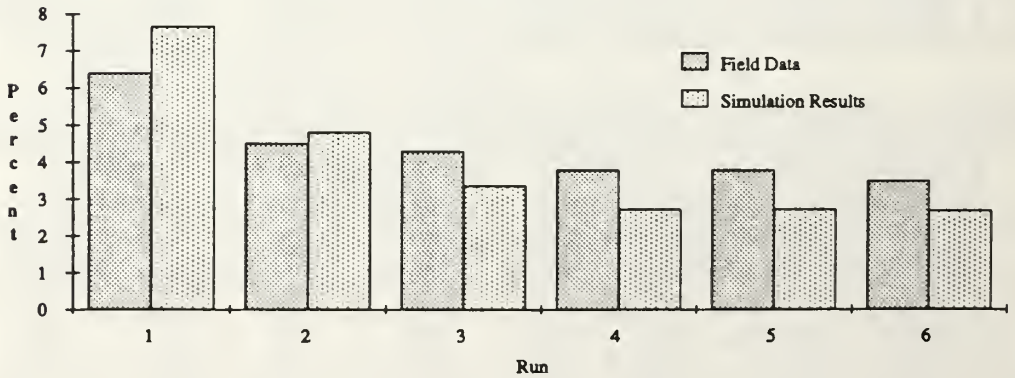

(c) Feeder 53

Fig. 20: Current THD relative to the fundamental for feeders 51 through 53

Referring to Tables 11–13, the simulated feeder 53 current fundamental is significantly smaller than the field measurements for all system configurations except run number four. The simulated feeder 51 and 52 current fundamentals are close to the measured values. Additionally, the simulated and measured harmonic currents and current THD are within a few percent in most cases and vary the most on feeder 52.

Perhaps the best overall indicator of the system modeling effectiveness is the comparison of measured and simulated voltage at the Audrain County 12.5 kV feeder trunk and the current supplied to the substation. Tables 14 and 15 summarize the voltage and current quantities at node two.

TABLE 14: VOLTAGE AT NODE 2—FIELD DATA AND SIMULATION RESULTS

Run	Fundamental (kV)		Fifth (% of Fund.)		Seventh (% of Fund.)		THD (% of Fund.)	
	Field Data	Simulation	Field Data	Simulation	Field Data	Simulation	Field Data	Simulation
1	12.57	12.60	0.50	1.13	0.40	0.29	0.84	1.16
2	12.47	12.53	0.32	0.68	0.60	0.49	0.81	0.84
3	12.47	12.46	0.23	0.47	0.62	0.62	0.92	0.78
4	12.43	12.42	0.21	0.40	0.59	0.50	0.78	0.64
5	12.45	12.38	0.20	0.37	0.40	0.39	0.62	0.54
6	12.44	12.31	0.17	0.30	0.18	0.20	0.56	0.36

TABLE 15: CURRENT AT NODE 2—FIELD DATA AND SIMULATION RESULTS

Run	Fundamental (Amperes)		Fifth (% of Fund.)		Seventh (% of Fund.)		THD (% of Fund.)	
	Field Data	Simulation	Field Data	Simulation	Field Data	Simulation	Field Data	Simulation
1	175.75	161.20	4.55	6.92	2.73	1.26	6.30	7.04
2	180.56	157.05	2.84	4.26	3.10	2.21	4.60	4.80
3	188.55	158.43	2.72	2.89	2.89	2.75	4.40	3.99
4	191.73	160.74	2.51	2.46	1.93	2.16	3.60	3.27
5	196.54	164.44	2.28	2.17	0.94	1.65	3.20	2.73
6	210.90	174.60	1.60	1.65	0.07	0.79	2.30	1.83

Figure 21 compares the simulated and measured current and voltage THD at node two, the Audrain County 12.5 kV feeder.

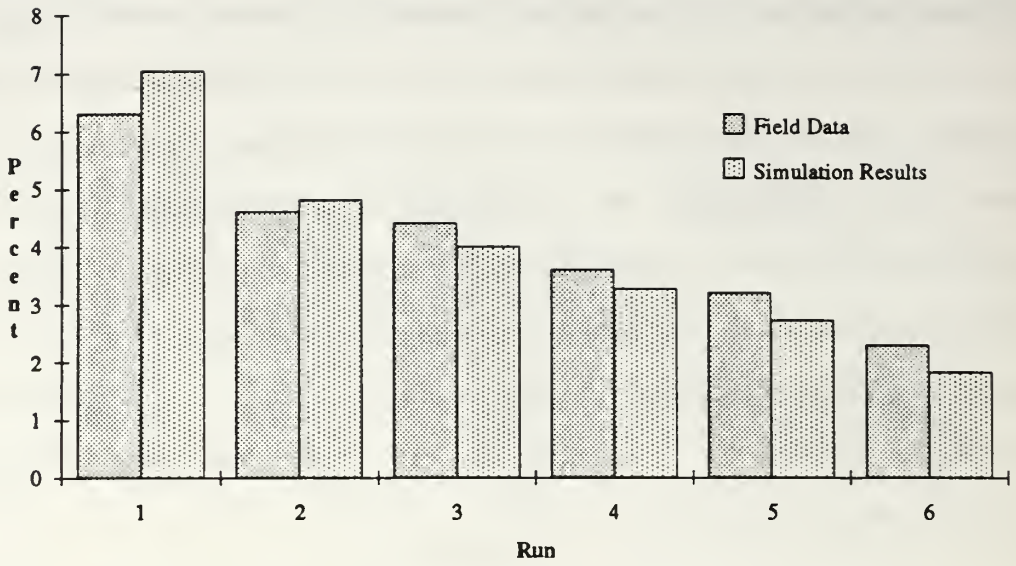

(a) Current THD at node 2

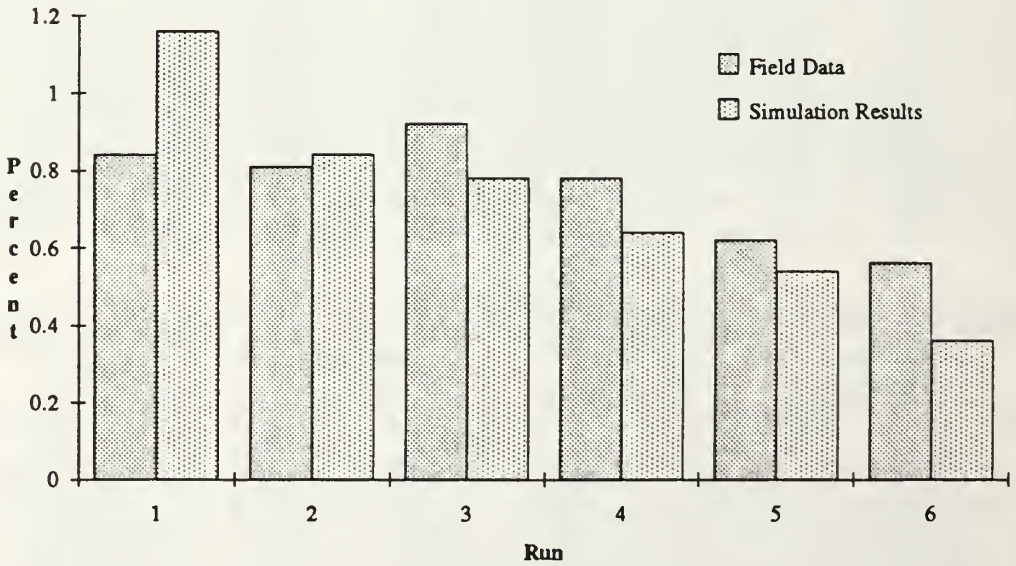

(b) Voltage THD at node 2

Fig. 21: Simulated and measured current and voltage THD at node 2

VI. MILITARY STANDARDS

The interface standard for shipboard systems, MIL–STD–1399 (NAVY) SECTION 300A of 13 October 1987, entitled *Electrical Power, Alternating Current (Metric)* provides guidance about power quality. Because of the assumptions and limitations of the *HARMFLO* program, comparisons between simulation results and the guidance provided by this standard to 400 Hz systems, current and voltage imbalances, and transient phenomenon are inappropriate.

Specific guidance that does apply to this study includes 5% maximum voltage THD, 3% maximum single voltage harmonic, and 5% maximum voltage deviation factor [20:pp. 8]. The voltage deviation factor is defined to be the maximum difference between the voltage waveform and a pure 60 Hz sine wave with amplitude equal to the maximum waveform value, relative to that maximum value [20:pp. 5].

Equipment must not induce single harmonic line currents greater than 3% of the full load rated fundamental for harmonic order between two and 32. If the power source characteristics are not specifically known, pulsed loads may not exceed 70 kVA. If the source characteristics are known, pulsed loads up to 25% of the generator rating may be used depending on the power factor. [20:pp. 15, 35]

Shipboard 60 Hz power distribution systems are designed to operate with power factors between 0.80 and 0.95. Although line-to-neutral filter capacitors are allowed, the preferred capacitor bank installation is line-to-line. In any case, installed capacitor banks may not exceed 0.1 μF for 60 Hz systems. Additionally, equipment rated at 5 kVA or more must use a three phase 440 V input and source impedances are assumed to be 5 Ω at 100–200 kHz unless specified otherwise. [20:pp. 14]

VII. CONCLUSIONS

Relatively little is known about the parameters used to describe the system of Fig. 1. However, most of the simulation results are remarkably close to the field measurements. The major disparities are the differences between simulated and measured current fundamental drawn by the customer and the current harmonics on feeder 52.

There are at least three possible reasons why the rectifier model for the seven 100 HP adjustable speed dc drives performs adequately with the test case and produces such a small current fundamental when connected to the entire system. A more detailed system model may be required to obtain the proper interaction between components. Another possibility is that the estimates of the customer's loads are inaccurate. Finally, the rectifier model internal to *HARMFLO* may not perform properly. Of the three, it is most likely that the system model requires more detail.

The disparity in current harmonics on feeder 52 is probably due to the fact that many household appliances produce harmonic currents. The system model does not include any nonlinear loads on feeder 52. Additionally, grouping residential loads to limit the system model size may be at the expense of accuracy.

The THD plots for the six system configurations show that there are system resonances and that *HARMFLO* simulations do predict system resonances with reasonable accuracy. The trends exhibited by the simulated and measured values are similar. Long line modeling and inclusion of some nonlinear loads on feeder 52 would likely improve results in this area.

From the military perspective, *HARMFLO* has apparent applications where large nonlinear loads are planned for shipboard installation. The design process for large

rectified loads would be enhanced by *HARMFLO* simulations, particularly since the parameters for such systems are more precisely known than the system of this study. Reference [20] should be updated to give more specific guidance about large rectified loads.

The Department of Defense (DoD) has chosen ADA as the preferred computer language for programs used by the DoD. Potential military users of *HARMFLO* should be aware that it is written in FORTRAN. Currently, there are no programs written in ADA with capabilities similar to *HARMFLO*.

APPENDIX
INPUT DATA SET FOR THE SYSTEM UNDER TEST

0001
AUDRAIN COUNTY MISSOURI. FEEDERS 51 - 53.
0002
SIMULATION OF AUDRAIN COUNTY DISTRIBUTION SYSTEM FOR
0002
COMPARISON TO FIELD DATA.
0002
ALL CAPACITORS CONNECTED
2003

1 swing bus01	0.000	0.000	0.000	0.000	0.000	100.000	0.0000
2 audrain 12kv03	0.000	0.000	0.000	0.000	0.000	0.000	0.0000
3 feeder 52-103	0.000	0.000	0.000	0.050	0.020	0.000	0.0000
4 feeder 52-203	0.000	0.000	0.000	0.120	0.060	0.000	0.0000
5 feeder 52-303	0.000	0.000	0.000	0.090	0.050	0.000	0.0000
6 feeder 52-403	0.000	0.000	0.000	0.090	0.050	0.000	0.0000
7 feeder 52-503	0.000	0.000	0.000	0.000	0.000	0.000	-0.6001
8 feeder 52-603	0.000	0.000	0.000	0.090	0.050	0.000	0.0000
9 feeder 52-703	0.000	0.000	0.000	0.020	0.010	0.000	0.0000
10 feeder 52-803	0.000	0.000	0.000	0.050	0.020	0.000	0.0000
11 feeder 51-103	0.000	0.000	0.000	0.390	0.190	0.000	-0.3001
12 feeder 51-203	0.000	0.000	0.000	0.050	0.020	0.000	0.0000
13 feeder 51-303	0.000	0.000	0.000	0.050	0.020	0.000	0.0000
14 feeder 51-403	0.000	0.000	0.000	0.050	0.020	0.000	0.0000
15 feeder 53-103	0.000	0.000	0.000	0.110	0.050	0.000	0.0000
16 feeder 53-203	0.000	0.000	0.000	0.000	0.000	0.000	-0.3001
17 feeder 53-303	0.000	0.000	0.000	0.220	0.100	0.000	0.0000
18 feeder 53-403	0.000	0.000	0.000	0.220	0.100	0.000	0.0000
19 feeder 53-503	0.000	0.000	0.000	0.000	0.000	0.000	-0.6001
20 feeder 53-603	0.000	0.000	0.000	0.290	0.140	0.000	0.0000
21 feeder 53-703	0.000	0.000	0.000	0.110	0.050	0.000	0.0000
22 feeder 53-803	0.000	0.000	0.000	0.040	0.020	0.000	0.0000
23 feeder 53-903	0.000	0.000	0.000	0.220	0.110	0.000	0.0000
24 feeder 53-1003	0.000	0.000	0.000	0.000	0.000	0.000	-0.6001
25 factorty 103	0.000	0.000	0.000	0.620	0.390	0.000	-0.3001
26 rect delta23	0.000	0.000	0.000	0.290	0.180	0.000	0.0000
27 rect wye23	0.000	0.000	0.000	0.210	0.130	0.000	0.0000

```
9999
0004
  1  2    0.00  94.00  0.00  0.00  0.00  0.00 0.000  0.0  0.000000
  2  3   25.00  50.00  0.00  0.00  0.00  0.00 0.000  0.0  0.000000
  2  0    0.00  94.00  0.00  0.00  0.00  0.00 0.000  0.0  0.000010
  3  4    8.00  15.00  0.00  0.00  0.00  0.00 0.000  0.0  0.000000
  4  5   22.00  43.00  0.00  0.00  0.00  0.00 0.000  0.0  0.000000
  5  6    9.00  18.00  0.00  0.00  0.00  0.00 0.000  0.0  0.000000
  6  7   22.00  44.00  0.00  0.00  0.00  0.00 0.000  0.0  0.000000
  7  8   22.00  44.00  0.00  0.00  0.00  0.00 0.000  0.0  0.000000
  8  9   45.00  88.00  0.00  0.00  0.00  0.00 0.000  0.0  0.000000
  9 10   20.00  40.00  0.00  0.00  0.00  0.00 0.000  0.0  0.000000
  2 11    9.00  18.00  0.00  0.00  0.00  0.00 0.000  0.0  0.000000
 11 12    5.00  10.00  0.00  0.00  0.00  0.00 0.000  0.0  0.000000
 12 13    8.00  15.00  0.00  0.00  0.00  0.00 0.000  0.0  0.000000
 13 14    9.00  29.00  0.00  0.00  0.00  0.00 0.000  0.0  0.000000
  2 15    2.00   3.00  0.00  0.00  0.00  0.00 0.000  0.0  0.000000
 15 16   15.00  29.00  0.00  0.00  0.00  0.00 0.000  0.0  0.000000
 16 17    5.00   9.00  0.00  0.00  0.00  0.00 0.000  0.0  0.000000
 17 18    4.00   7.00  0.00  0.00  0.00  0.00 0.000  0.0  0.000000
 16 19   10.00  20.00  0.00  0.00  0.00  0.00 0.000  0.0  0.000000
 19 20   10.00  20.00  0.00  0.00  0.00  0.00 0.000  0.0  0.000000
 20 21   10.00  20.00  0.00  0.00  0.00  0.00 0.000  0.0  0.000000
 21 22   39.00  75.00  0.00  0.00  0.00  0.00 0.000  0.0  0.000000
 22 23   15.00  29.00  0.00  0.00  0.00  0.00 0.000  0.0  0.000000
 19 24    2.00   3.00  0.00  0.00  0.00  0.00 0.000  0.0  0.000000
 24 25    0.00   0.01  0.00  0.00  0.00  0.00 0.000  0.0  0.000000
 25 26    0.00   0.01  0.00  0.00  0.00  0.00 0.000  0.0  0.000000
 25 27    0.00   0.01  0.00  0.00  0.00  0.00 0.000  0.0  0.000000
9999
0012
 26  15.35  543.78   0.00   0.00       0.06600  30.00
 27  11.51  407.84   0.00   0.00       0.04100   0.00
9999
0005
0 0 7 0 0 0 0 0 1 0 0 0 0 2 0 0 2 0
0015
```

LIST OF REFERENCES

[1] Kevin C. Simpson, "The effects of harmonic distortion in today's electrical networks," *76th Annual Meeting. Technical Section. Canadian Pulp and Paper Association,* pp. 405–13, Canadian Pulp and Paper Assoc, Montreal, Que., Canada, January 1990.

[2] G.T. Heydt, W.M. Grady, and D. Xia, "Harmonic Power Flow Studies Volume 1: Theoretical Basis," Research Report EL–3300–CCM Volume 1, Electric Power Research Institute, Palo Alto, California, November 1983.

[3] M.F. McGranaghan, R.C. Dugan, Jack A. King, and W.T. Jewell, "Distribution feeder harmonic study methodology," *IEEE Trans. on Power Apparatus and Systems,* Vol. PAS–103, No. 12, pp. 3663–3671, December 1984.

[4] Stephen M. Williams, "The Propagation and Mitigation of Harmonics Generated by Power Electronic Loads on an Electric Distribution System," Ph.D. dissertation, University of Missouri-Columbia, 1990.

[5] William D. Stevenson, Jr., *Elements of Power System Analysis,* McGraw–Hill Book Company, New York, 1982.

[6] IEEE Std 519–1981, *IEEE Guide for Harmonic Control and Reactive Compensation of Static Power Converters,* IEEE, New York, April 1981.

[7] Elham B. Makram, Adly A. Girgis, and Katherine P. Thornton, "Transient analysis of capacitor switching in unbalanced distribution system with harmonic distortion," *Electric Machines and Power Systems,* Vol. 17, pp. 75–92, 1989.

[8] Robert D. Strum and Donald E. Kirk, *First Principles of Discrete Systems and Digital Signal Processing,* pp. 802-807, Addison-Wesley, Reading, Massachusetts, 1989.

[9] IEEE Course Text 84 EHO221–2–PWR, *Power System Harmonics,* Edited by A.A. Mahmoud, W.M. Grady, and M.F. McGranaghan, IEEE, New York, 1984.

[10] Lynda K. Ell and Earl Council, "Open–circuit harmonic distortion on in–service distribution transformers," *Proceedings on Power Quality,* Vol. 17, No. 1, pp. 13–19, Electric Power Systems Research, October 1989.

[11] John Curlett, "Effective solutions for harmonic problems from single phase, nonlinear loads," *Official Proceedings of the First International Conference on Power Quality,* pp. 317–23, Intertec Commun, Ventura, CA, October 1989.

[12] Ned Mohan, Tore M. Undeland, and William P. Robbins, *POWER ELECTRONICS: Converters, Applications, and Design,* John Wiley & Sons, New York, 1989.

[13] G.T. Heydt, W.M. Grady, and D. Xia, "The HARMFLO Code: Version 4.0 User's Guide," Research Report EL–4920–CCM, Electric Power Research Institute, Palo Alto, California, November 1986.

[14] Kendall E. Atkinson, *An Introduction to Numerical Analysis,* John Wiley & Sons, New York, 1978.

[15] D. Xia and G.T. Heydt, "Harmonic Power Flow Studies Part I—Formulation and Solution," *IEEE Trans. on Power Apparatus and Systems,* vol. PAS–101, no. 6, pp. 1257–1265, June 1982.

[16] D. Xia and G.T. Heydt, "Harmonic Power Flow Studies Part II—Implementation and Practical Application," *IEEE Trans. on Power Apparatus and Systems,* vol. PAS–101, no. 6, pp. 1266–1270, June 1982.

[17] J. Arrillaga and C.P. Arnold, *Computer Analysis of Power Systems,* John Wiley & Sons, Chichester, England, 1990.

[18] Anthony J. Pansini, *Electrical Distribution Engineering,* McGraw–Hill Book Company, New York, 1983.

[19] Martin A. Plonus, *Applied Electromagnetics,* McGraw–Hill Book Company, New York, 1978.

[20] Department of the Navy Military Specification MIL–STD–1399(NAVY) SECTION 300A, *Electric Power, Alternating Current(Metric), Interface Standard for Shipboard Systems,* 13 October 1987.

INITIAL DISTRIBUTION LIST

1. Defense Technical Information Center — 2
   Cameron Station
   Alexandria, VA 22304–6145

2. Library, Code 52 — 2
   Naval Postgraduate School
   Monterey, CA 93943–5002

3. Chairman, Code EC — 1
   Department of Electrical and Computer Engineering
   Naval Postgraduate School
   Monterey, CA 93943–5000

4. Professor Stephen M. Williams, Code EC/Wl — 1
   Department of Electrical and Computer Engineering
   Naval Postgraduate School
   Monterey, CA 93943–5000

5. Professor Murali Tummala, Code EC/Tu — 1
   Department of Electrical and Computer Engineering
   Naval Postgraduate School
   Monterey, CA 93943–5000

6. Commanding Officer — 1
   Naval Sea Systems Command (Code 56)
   Washington, DC 20362–5101

7. Commanding Officer — 1
   Naval Sea Systems Command (Code 56Z)
   Washington, DC 20362–5101

8. David Taylor Research Center — 1
   Attn: David Clayton
   Annapolis Lab (Code 2714)
   Annapolis, MD 21402–5067

9. Stephen M. Gedo Sr. — 1
   2100 Springdale Boulevard #Y106
   Palm Springs, FL 33461

10. LT Christopher N. Gedo — 2
    U.S. Naval Ship Repair Facility
    Box 34
    FPO San Francisco, CA 96651–1400

Thesis
G25753 Gedo
c.1 Computer analysis of harmonic distortion in electrical power distribution systems.